

## Exciton dressing and capture by a photonic band edge

Shengjun Yang and Sajeev John

*Department of Physics, University of Toronto, 60 St. George Street, Toronto, Ontario, Canada M5S 1A7*

(Received 22 March 2007; revised manuscript received 27 May 2007; published 28 June 2007)

We demonstrate electromagnetically induced anomalous quantum dynamics of an exciton in a photonic band gap (PBG)-quantum well (QW) heterostructure. Within the engineered electromagnetic vacuum of the PBG material, the exciton can propagate through the QW by the emission and reabsorption of virtual photons in addition to the conventional electronic hopping mechanism. When the exciton wave vector and recombination energy nearly coincide with a photonic band edge, the exciton kinetic energy is lowered by 1–10 meV through coherent radiative hopping. This capture of the exciton by the photonic band edge is accompanied by strong electromagnetic dressing in which exciton's renormalized effective mass is 4–5 orders of magnitude smaller than in the absence of the PBG environment. This dressed exciton exhibits a long radiative lifetime characteristic of a photon-atom bound state and is robust to phonon-assisted recombinative decay. By inheriting properties of the PBG electromagnetic vacuum, the bound electron-hole pair becomes a stable, ultramobile quantum excitation.

DOI: [10.1103/PhysRevB.75.235332](https://doi.org/10.1103/PhysRevB.75.235332)

PACS number(s): 73.21.-b, 42.70.Qs, 42.50.-p, 71.36.+c

### I. INTRODUCTION

Photonic band gap (PBG) materials<sup>1,2</sup> are artificial periodic dielectrics in which light over a certain frequency range cannot propagate. In the presence of engineered defects (deviations from periodicity) or random disorder, PBG materials exhibit the striking phenomenon of light localization.<sup>3</sup> Another fundamental property of PBG materials is the frequency selective control of atomic spontaneous emission through engineering of the electromagnetic vacuum.<sup>4–7</sup> In the case of stationary two-level atoms or quantum dots embedded in three-dimensional (3D) PBG materials, a variety of novel effects in quantum electrodynamics are predicted. Among these is the emergence of coherent dipole-dipole interaction between nearby resonant atoms.<sup>8–10</sup> This becomes the dominant radiative process when single-photon spontaneous emission is suppressed<sup>2,11</sup> by the PBG. While previous studies of quantum electrodynamics have focused on stationary light emitters, semiconductor structures may host mobile excitations consisting of bound electrons and holes. Excitons in bulk solids<sup>12</sup> and semiconductor quantum well (QW) structures<sup>13,14</sup> have a long and rich history. Emission and absorption of light by excitons are governed not only by energy conservation but also by momentum conservation. The interplay between exciton motion and radiative dynamics leads to unexpected consequences in the engineered electromagnetic vacuum of a PBG material.

In the past decade, there have been important investigations of Bose-Einstein statistics of excitons in semiconductor microcavities. In this context, the microcavity typically consists of a QW (or multiple QWs) sandwiched above and below by dielectric mirror stacks. Experimental studies of exciton and cavity photon interaction have shown striking effects of Bose quantum statistics such as stimulated scattering and amplification.<sup>15–18</sup> However, due to the one-dimensional (1D) nature of the mirror stacks and the low dielectric contrast between mirror layers, only a small stop gap along one direction is available for the confinement of light. This cavity photonic mode is a leaky mode that couples

to the electromagnetic continuum of modes in the external vacuum. Unless the cavity quality factor is extremely high, the limited confinement of light by this effective 1D PBG material enhances the photon emission rate in the direction normal to the QW, thereby decreasing the exciton lifetime for radiative recombination. The exciton lifetime can be prolonged by use of a double quantum well layer in which the electron and hole wave functions are separated. However, this leads to weaker coupling of the exciton dipole to electromagnetic modes. In addition, a membrane containing a thin QW layer and patterned with air holes in a 2D photonic crystal slab (PCS) has recently been studied by Andreani *et al.*<sup>19</sup> The guided mode in PCS is not strongly confined, and there is no full 3D band gap to inhibit the single-photon spontaneous emission of an exciton. In contrast, the PBG environment in our proposed heterostructure provides the possibility of simultaneous strong coupling between exciton and photon as well as long exciton lifetime.

In this paper, we consider the detailed interplay between exciton charge carrier dynamics and strongly confined photons in the engineered electromagnetic vacuum of a 3D PBG heterostructure. This heterostructure consists of a thin single layer quantum well sandwiched above and below by 3D PBG materials. The QW acts as a planar defect that induces guided optical modes within the otherwise forbidden 3D PBG. When the electron-hole recombination energy lies within the PBG, the exciton cannot decay without recourse to additional mechanisms involving phonons, impurities, or other recombination centers. Instead, the exciton forms a bound state with the photon it would normally emit. Unlike the stationary photon-atom bound state,<sup>4,5</sup> the bound exciton-photon can propagate through the quantum well at a fixed in-plane wave vector. If the exciton recombination energy and in-plane wave vector nearly coincide with a photonic band edge, strong-coupling effects provide up to a 10 meV reduction in the exciton energy. This leads to exciton dynamics and facilitates quantum coherent behavior of excitons at up to 100 K in the engineered electromagnetic vacuum.

In our 3D PBG heterostructure containing a QW defect layer, planar guided optical modes appear within the photo-

nic band gap. By careful choice of structural parameters, it is possible to confine the 2D guided modes within a spectral range that occupies only part of the original 3D PBG. By choosing the photonic crystal lattice constant appropriately, we can place the exciton radiative recombination energy near resonance with either (i) the two-dimensional (2D) band edge of the planar guided modes within the 3D PBG, (ii) the upper 3D band edge of the bulk photonic crystal (in which the exciton energy may also coincide with one of the 2D guided modes), or (iii) the lower 3D band edge of the bulk photonic crystal.

When the exciton interacts nearly in resonance with any of the above electromagnetic modes, mutual exchange of energy between charge carriers and photon leads to a normal mode splitting analogous to vacuum Rabi splitting in a stationary atom.<sup>4-6</sup> If the exciton interacts strongly with the 3D upper band edge, it can lower its kinetic energy considerably through the coherent process of recombinative decay at one position, emission of a nonresonant virtual photon outside the 3D PBG, and re-excitation at another position through reabsorption of the virtual photon. This process is analogous to coherent resonance dipole-dipole interaction (RDDI) between a pair of nearby impurity atoms.<sup>20</sup> RDDI in PBG materials has been shown to provide unusual cooperative behavior among two-level atoms.<sup>8,9</sup> In the context of a mobile, electron-hole bound state, this coherent radiative hopping provides an alternative mechanism for exciton transport that, for certain energies and wave vectors, dominates traditional electronic hopping. Through this electromagnetic hopping and normal mode splitting, the exciton inherits certain features of the photonic bands. In particular, the exciton energy-momentum relation is fundamentally changed in the vicinity of the photonic band-edge wave vector. The exciton and photon system exhibits a qualitatively different ground state with a lowered energy and reduced effective mass at the photonic band edge. In the presence of small thermal fluctuations or scattering processes, an exciton of any initial wave vector is captured in this dressed state by the corresponding photonic band edge. Unlike conventional exciton-polariton states based on coupling to a 1D optical cavity, long lifetime and strong coupling emerge simultaneously and robustly in the 3D PBG heterostructure.

This paper is organized as follows. In Sec. II, we give a general description of the photonic band gap heterostructure containing a quantum well. We then present a simplified model of the photonic modes including planar guided modes, extended 3D modes, and the QW exciton Hamiltonian. In Sec. III, we describe a general interaction Hamiltonian for the QW exciton and the structured electromagnetic reservoir. By applying a canonical transformation to this interaction Hamiltonian, we provide a simple physical picture of the exciton radiative hopping mechanism. We then present detailed results for the three different exciton-photonic band-edge interactions listed above. In Sec. V, we briefly discuss the robustness of the renormalized exciton to decay mediated by longitudinal optical (LO) phonons. We also discuss the robustness of exciton capture by the photonic band edge to static disorder. A microscopic derivation of the interaction Hamiltonian for the QW exciton with electromagnetic modes of the photonic band gap heterostructure is given in the Appendix.

## II. MODEL OF EXCITONS AND PHOTONS IN A PBG QUANTUM WELL

For concreteness, we consider a single layer of QW sandwiched by 3D PBG materials made from either a square spiral<sup>21</sup> or a woodpile<sup>22</sup> architecture. Both heterostructures exhibit similar optical characteristics. The background PBG material is assumed to have dielectric constant of silicon ( $\epsilon = 11.9$ ) and may consist of polycrystalline<sup>23-25</sup> or crystalline<sup>26,27</sup> semiconductor. On the other hand, the thin quantum well layer is assumed to be a high quality crystalline semiconductor made from well-studied III-V compounds, such as GaAs or InGaAsP. Such a quantum well heterostructure has recently been fabricated by Noda *et al.*<sup>28</sup> Here, a flat light-emitting layer composed of three InGaAsP multiple quantum wells with emission wavelength around  $1.5 \mu\text{m}$  was inserted in the middle of the GaAs 3D woodpile structure with one unit cell above and below. A heterostructure of this type could be adapted for the study of anomalous exciton dynamics proposed in this paper. This requires increasing the number of layers of PBG material above and below to inhibit the exciton radiative decay and engineering the lattice constant to set the exciton recombination energy in resonance with a specific photonic band edge. Figures 1(a) and 1(b) illustrate a QW layer sandwiched between a pair of woodpile<sup>25,29,30</sup> PBG materials and its corresponding band structure for our proposed heterostructure. The QW can also be grown in silicon-based structures by introducing a buffer region between QW and the PBG cladding regions. The dielectric constants of common QW layers are on the order of 10 and the exciton recombination energy is on the order of 1 eV. We assume that exciton recombination energy and the PBG are in the transparency region of the underlying semiconductor materials. Our proposed geometry for QW insertion consists of separating the two halves of a bulk PBG material by the thickness of the QW and then placing the solid semiconductor crystal layer in the resulting air gap. For the purpose of specific illustration and potential linkage to optical communication application, we consider QW with dielectric constant of 11.9 with an exciton whose recombination energy corresponds to a photon of wavelength of  $1.5 \mu\text{m}$ .

### A. Band structure of QW-PBG heterostructure

We begin by evaluating the electromagnetic mode structure for the PBG-QW heterostructure. Plane wave expansion (PWE) method is used to calculate the band structure in a supercell consisting of four unit cells of square spiral PBG material above and below the QW [see Fig. 2(a)]. Figure 2(b) shows the photonic band structure for a QW thickness of 6% of the lattice constant of the 3D photonic crystal. For a 3D PBG centered at  $1.5 \mu\text{m}$ , the actual lattice constant  $a = 550 \text{ nm}$  for direct square spiral 1.<sup>31</sup> The QW thickness in this case is slightly less than 33 nm. The square spiral structural parameters are given in the caption of the Fig. 2(b). Two gray regions represent the original Bloch photonic modes of the bulk 3D PBG material without any defect. Two planar guided band solid lines (red online) remain within the PBG as the supercell size is increased. If the QW thickness is

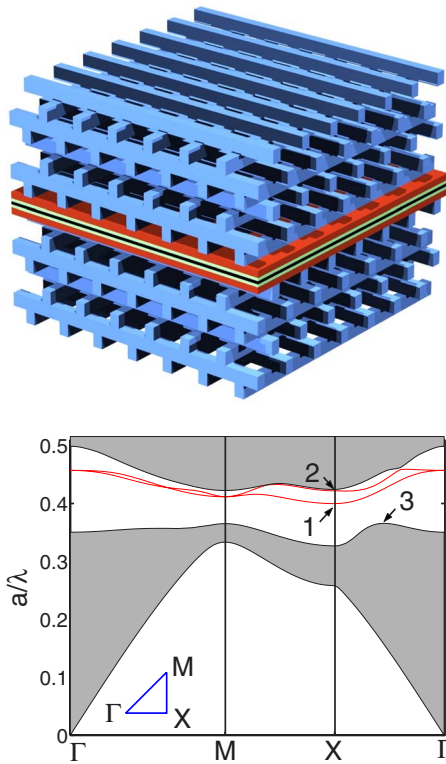


FIG. 1. (Color online) (a) PBG-QW (quantum well) heterostructure, consisting of a QW layer sandwiched by woodpile structure. The 3D woodpile structure is cut into two halves at the interface between two orthogonal dielectric rod layers, the halves are separated, and the QW inserted. The dielectric rods have a rectangular cross section with width  $0.25a$  and height  $0.3a$ , where  $a$  is the center to center distance between adjacent rods in the same layer. One unit cell of the woodpile consists of four stacking layers. Accordingly, the periodicity is  $1.2a$  along the stacking direction. (b) The corresponding photonic band structure calculated by supercell plane wave expansion (PWE) method. The supercell consists of a defect of thickness  $0.06a$  sandwiched by four unit cells of woodpile structure above and four unit cells of woodpile structure below. Shaded regions show allowed bands in the 3D woodpile cladding region. Solid (red) curves in upper white region (PBG) are planar guided modes induced by QW defect. Labeled are the planar band edge (1), the upper 3D band edge (2), and the lower 3D band edge (3).

increased, more planar guided modes enter the original 3D PBG. At a critical QW thickness of  $0.1a$ , the entire 3D PBG is filled with 2D guided modes. For the purpose of illustrating various exciton-photonic band-edge interactions, we limit the QW thickness so that a complete 3D PBG remains open in the vicinity of the planar defect. For 2D guided modes, the electromagnetic field is exponentially localized in the  $z$  direction and confined near the QW. Light in these modes can propagate only along the QW plane. Other modes merge into the continuum (gray region) as the supercell size is increased. We interpret these as bulk 3D bands for an infinite crystal containing a single QW layer. This type of electromagnetic mode structure is a generic feature of the PBG-QW heterostructures.

An alternative approach to planar exciton confinement within a 3D PBG material (fabricated from single-crystal

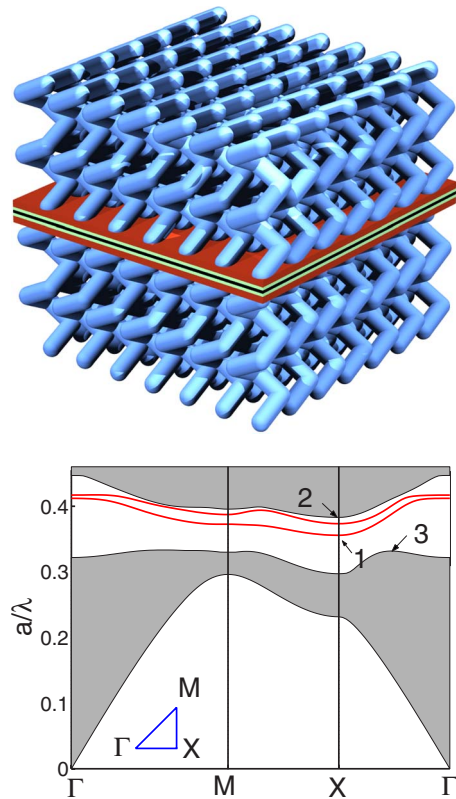


FIG. 2. (Color online) (a) PBG-QW (quantum well) heterostructure consisting of a QW layer sandwiched by the direct square spiral structure (DSS) (Refs. 21 and 31). The original 3D PBG material is cut into two halves at the bottom of one unit cell, the halves are separated, and the QW inserted. The unit cell of PBG material is a DSS:1 structure (Ref. 31) consisting of the interleaving, square spiral arms with a transverse arm length of  $0.7a$ , vertical period of  $1.35a$ , and circular cross section of  $0.2a$ , where  $a$  is the lattice constant. The square spiral arms wind in phase with each other and are arrayed on a 2D square lattice. (b) The corresponding photonic band structure calculated by supercell plane wave expansion (PWE) method. The supercell consists of a defect of thickness of  $0.06a$  sandwiched by four unit cells of PBG material above and four unit cells of PBG material below. Shaded regions show allowed bands of the 3D PBG cladding regions. Solid (red) curves in upper white region (PBG) correspond to planar guided modes induced by QW defect. Labeled are the planar guided band edge (1), the upper 3D band edge (2), and the lower 3D band edge (3).

semiconductor) consists of retaining the bulk photonic crystal geometry throughout. This alternative architecture involves introducing a compositional change in the backbone semiconductor contained within a thin planar region. In this case, the QW would not consist of a solid plane of material but would contain a periodic array of solid-to-air interfaces wherever the QW plane cuts the 3D PBG backbone. This architecture maintains the large 3D PBG of the cladding regions throughout the heterostructure. Such structures have also been fabricated recently.<sup>28,32</sup> Here, a light-emitting layer containing a high quality thin (50 nm) layer of multiple quantum well (MQW) made from III-V semiconductor material (InGaAsP/InP) within woodpile structure (GaAs) in the range of  $1.55 \mu\text{m}$  was fabricated. The light-emitting

layer is simply a planar compositional change within the woodpile structure. However, the large number of dielectric surfaces may provide unwanted exciton recombination centers.

In order to prevent exciton recombination at dielectric to air interfaces, it may also be suitable to embed a layer of quantum dots into a 3D PBG material rather than using periodically pierced QW layers. In this case, the bare exciton is confined to the quantum dots and is immobile. However, the dressed exciton may still acquire a high mobility through radiative processes in which it is transported from one quantum dot to another by emission and reabsorption of virtual photons. This is analogous to resonance dipole-dipole interaction between stationary atoms in a PBG material.<sup>4,5</sup>

In this paper, we limit our study to a solid QW sandwiched by separated halves of semi-infinite PBG material attached on either side. The resulting electromagnetic modes can be inferred from a supercell PWE calculation and examining the field patterns. We focus on exciton-photon strong-coupling regions related to three band edges, indicated by numbers in Figs. 1(b) and 2(b). In order to first illustrate the physics with analytical results, we adopt a simple effective-mass approximation for the photonic dispersion around these band edges, valid when the exciton recombination energy occurs close to the band edge. It is straightforward to treat realistic photonic dispersion relations for all  $\vec{k}$  vectors. This is done subsequently by numerical calculation.

The photonic dispersion near each band edge is parametrized in the effective-mass approximation as

$$\omega_{\vec{q},k_z}^{(i)} = \omega_i + \frac{ac}{2\pi} [A_x^{(i)}(q_x - q_x^{(i)})^2 + A_y^{(i)}(q_y - q_y^{(i)})^2 + A_z^{(i)}(k_z - k_i)^2], \quad i = 1, 2, 3. \quad (1)$$

Here,  $\omega_i$  is the band-edge frequency of the  $i$ th band ( $i=1$ , planar guided mode;  $i=2$ , upper 3D band-edge mode; and  $i=3$ , lower 3D band-edge mode) and  $(q_x^i, q_y^i, k_i)$  is the wave vector position of band edge  $\omega_i$ .  $a$  is the 3D photonic crystal lattice constant and  $c$  is the speed of light in vacuum.  $A_x^{(i)}$  and  $A_y^{(i)}$  are dimensionless 2D effective-mass parameters along the  $x$  and  $y$  directions, respectively, extracted from realistic photonic band structure calculation. Similarly,  $A_z^{(i)}$  is a dimensionless effective-mass parameter describing photonic dispersion in the  $z$  direction (normal to QW) as obtained by PWE method. For the upper 3D band edges shown in Figs. 1(b) and 2(b),  $A_z^{(2)} > 0$ , whereas the lower 3D band edge exhibits negative effective mass,  $A_z^{(3)} < 0$ . Since the planar guided photon has dispersion only along the QW plane, it follows that  $A_z^{(1)} = 0$ .

The electric field amplitude of a general Bloch mode photon at wave vector  $[\vec{q} \equiv (q_x, q_y), k_z]$  can be written as

$$\vec{E}_{\vec{q},k_z}(\vec{r}) = \vec{u}(\vec{\rho}, z) e^{i(\vec{q} \cdot \vec{\rho} + k_z z)} = \sum_n \vec{u}_{G_{\parallel}^n}(\vec{\rho}, z) e^{i[(\vec{q} + G_{\parallel}^n) \cdot \vec{\rho} + k_z z]}, \quad (2)$$

where  $\vec{r} \equiv (\vec{\rho}, z)$ ,  $\vec{\rho}$  is the in-plane coordinate vector, and  $\{G_{\parallel}^n\}$  are the 2D reciprocal wave vectors. The function  $\vec{u}_{G_{\parallel}^n}$  is defined below for different spectral ranges.

In the case of a planar guided mode ( $i=1$ ),  $\vec{u}(\vec{\rho}, z)$  is a function confined in the  $z$  direction around the QW plane and periodic along the QW plane with  $k_z=0$ . For 3D extended Bloch modes ( $i=2, 3$ ),  $\vec{u}(\vec{\rho}, z)$  is a periodic function in the coordinate  $\rho$ , but also extended in the  $z$  direction. The wave function in each case is normalized in the supercell. In order to verify the accuracy of the electric field pattern in the QW obtained by supercell PWE, we use the finite difference time domain (FDTD) method with a resolution of 50 points per lattice constant  $a$  in each directions. At this resolution, a planar dielectric defect with thickness of  $0.06a$  can be represented by three layers of FDTD mesh points. In our supercell, we insert the planar dielectric defect material precisely in the middle with four unit cells of periodic PBG material on either side. The QW is situated in the middle of this planar dielectric defect. This means that the confined exciton feels the electric field generated in the second layer of the FDTD mesh points in the defect.

The task of obtaining highly accurate field patterns for the unconfined 3D band-edge modes in the QW layer calculated from supercell is more challenging. These modes are not localized in the  $z$  direction and they evolve slowly to the bulk photonic crystal band edges as the supercell size increases. Indeed, the field distribution in the QW for these modes may be influenced by sample boundary conditions many unit cells away from the QW itself. Rather than treating this variability with specific sample boundary conditions, we adopt a simple modification of the bulk 3D band-edge modes for the infinite periodic 3D crystal (without QW) as a typical field pattern for the actual sample containing the QW. More specifically, we use a suitably screened (by the dielectric constant of the QW) version of the Bloch field pattern of the bulk 3D band-edge modes as our model field pattern in evaluating exciton-photon interaction in the QW.

From our calculation of the planar guided band field patterns using high resolution FDTD, we find that the QW layer screens the normal component of an applied electric field by acquiring surface polarization charges. This is consistent with the field boundary condition in which the displacement field is continuous along the normal direction and the electric field is continuous along the tangential direction. In adapting the 3D band-edge modes to the QW layer, we assume that the only major modification of these modes to the QW architecture is a simple dielectric screening effect on the  $z$  component of the electric field. Due to the large dielectric constant of the quantum well layer, the dominant contributions to the exciton-photon interaction come from larger, un-screened, in-plane electric field components of the Bloch mode.

## B. Quantum well exciton model

In the electronic, two-band (conduction and valence bands) effective-mass approximation, the QW exciton wave function, polarized in the  $j$  direction, in its lowest bound state, with an in-plane wave vector  $\vec{q}$ , is described by the wave function<sup>33</sup>

$$|\Psi_{j,\vec{q}}\rangle = B_{j,\vec{q}}^\dagger |0\rangle = \sum_{\vec{k}} A_{\vec{k},\vec{q}} a_{\vec{q}/2+\vec{k}}^\dagger b_{\vec{q}/2-\vec{k}}^\dagger |0\rangle, \quad (3a)$$

$$A_{\vec{k},\vec{q}} = \int d\vec{\rho} \phi(\rho) \frac{e^{-i[\vec{k}+(m_h^*-m_e^*)/(m_h^*+m_e^*)(\vec{q}/2)]\cdot\vec{\rho}}}{\sqrt{S}}, \quad (3b)$$

$$\phi(\rho) = \left(\frac{8}{\pi a_B^2}\right)^{1/2} \exp\left(-\frac{2\rho}{a_B}\right). \quad (3c)$$

Here,  $m_e^*$  and  $m_h^*$  are the effective masses of electron and hole, respectively.  $a^\dagger$  and  $b^\dagger$  are the creation operators for the electron and hole, respectively.  $B_{j,\vec{q}}^\dagger$  is the creation operator for the exciton, where  $j$  is the exciton polarization index (to be explained below),  $\vec{q}$  is the total center-of-mass, in-plane momentum of the exciton, and  $\vec{\rho}$  is the in-plane displacement vector between the electron and hole.  $A_{\vec{k},\vec{q}}$  is the Fourier transform of the electron-hole relative motion wave function  $\phi(\rho)$ , which is assumed to take a form of a  $1s$  state (2D hydrogenic orbital) describing the ground state of the bound exciton.  $a_B$  is the Bohr radius of a hydrogenic 3D exciton. For a pure 2D exciton, the actual radius is reduced to  $a_B/2$ . Assuming an infinite barrier potential at the upper and lower surfaces of the thin QW layer, the single particle state created by  $a^\dagger$  or  $b^\dagger$  can be written in the envelope function approximation as

$$\psi_{(c,v),\vec{k},m}(\vec{\rho}',z) = \frac{\exp(i\vec{k}\cdot\vec{\rho}')}{\sqrt{S}} f_{(c,v),m}(z) u_{\Gamma(c,v)}(\vec{\rho}',z), \quad (4a)$$

$$f_{(c,v),m}(z) = \left(\frac{2}{l_w}\right)^{1/2} \sin\left(\frac{m\pi z}{l_w}\right). \quad (4b)$$

Here,  $S$  and  $l_w$  are the QW area and thickness, and  $\vec{\rho}'$  and  $z$  are the in-plane displacement vector and the normal displacement coordinate of the electron (or the hole), respectively.  $u_{\Gamma(c,v)}(\vec{\rho}',z)$  is the electronic Bloch function taken at the  $\Gamma$  point in the electronic Brillouin zone of the conduction band or valence band.  $f_{(c,v),m}(z)$  are envelope functions of the electron or the hole in the  $z$  direction normal to the QW. In the following, we set  $m=1$  in Eq. (4b) to obtain the lowest energy exciton manifold and drop the index  $m$  in subsequent discussions.

The exciton exhibits a polarization degree of freedom resulting from the different symmetries (within the electronic unit cell) of the microscopic electronic Bloch functions,  $u_{\Gamma(c,v)}(\vec{\rho}',z)$  shown in Eq. (4a). In the detailed derivation of the exciton-photon interaction Hamiltonian given by Eq. (A14a) in the Appendix, the optical dipole transition matrix element,  $\vec{d} = \langle u_{\Gamma_c}(\vec{r}) | e\vec{r} | u_{\Gamma_v}(\vec{r}) \rangle$ , that creates the exciton can fall along one of the three independent directions. The orientation of the dipole is determined by the symmetry of the underlying atomic orbitals that constitute the electronic Bloch functions. For example, an optical transition from a valence band state with a large  $s$  component (zero orbital angular momentum) to a conduction band state with large  $p_i$  component,  $i=x,y,z$  (angular momentum  $\hbar$ ), provides excitonic polarization in the  $x$ ,  $y$ , and  $z$  directions, respectively. This leads to three distinct types of excitons labeled as T, L, and Z excitons, respectively (see the Appendix for precise definition). If the QW is placed in a featureless electromag-

netic vacuum (no PBG cladding material), the T exciton couples to free space TE modes (electric field vector is perpendicular to the "plane of incidence," which contains the input beam, the output beam, and the direction normal to the sample surface). The L exciton couples to free space TM modes (magnetic field vector is perpendicular to the plane of incidence). The Hamiltonian for such a featureless electromagnetic vacuum separates for different exciton polarizations. Since the actual photonic modes in the PBG-QW heterostructure have a mixed polarization structure, the T, L, and Z excitons in this engineered vacuum are all coupled. However, due to the screened electric field normal to the planar defect, the photon-Z-exciton coupling is comparatively weak. We consider only the T and L excitons in what follows. We make a further approximation in the case of an exciton resonantly coupled to the planar guided mode. For the planar guided band edge, our numerical results show that the electric field is strongly polarized perpendicular to the band-edge wave vector at which the exciton is captured. Accordingly, we only consider the T-exciton-planar guided mode interaction. For the 3D band-edge modes, the planar electric fields along the transverse and longitudinal directions are comparable. Therefore, we consider both T and L excitons in our exciton-3D band-edge interaction models.

### III. EXCITON-PHOTON COUPLING IN A PHOTONIC CRYSTAL

The construction of a model Hamiltonian for exciton-photon coupling in a PBG environment is simplified by energy and momentum conservation considerations.<sup>12</sup> In a QW with continuous translational symmetry in the plane, momentum is conserved. This implies that an exciton with in-plane wave vector  $\vec{q}$  cannot undergo purely (one-photon) radiative decay unless it emits a photon with the same  $\vec{q}$ . In general, this leads to the requirement for defects that act as recombination centers for radiative decay to occur. When the quantum well is sandwiched above and below by 3D PBG material, this continuous translational symmetry is replaced by the discrete translational symmetry imposed by coupling to Bloch mode photons (see the Appendix). This discrete symmetry is characterized by the set of reciprocal lattice vectors  $\{G_{\parallel}^n\}$  for the 3D photonic crystal parallel to the QW plane. This implies that an exciton of wave vector  $\vec{q} + G_{\parallel}^n$  can also recombine to emit a photon of wave vector  $(\vec{q}, k_z)$  is in the first Brillouin zone of the photonic crystal. The QW breaks translational symmetry in the  $z$  direction. Consequently, a photon with arbitrary  $z$  component  $k_z$  can be emitted provided that such a photon exists near the recombination energy. A microscopic derivation of the exciton-photon coupling, taking into account the properties described above, is given in the Appendix. The resulting model Hamiltonian (under rotating wave approximation) can be written as

$$H = H_{exc} + H_{EM} + H_i, \quad (5a)$$

$$H_{exc} = \sum_{j,n} \varepsilon_{j,\vec{q}+G_{\parallel}^n} B_{j,\vec{q}+G_{\parallel}^n}^\dagger B_{j,\vec{q}+G_{\parallel}^n}, \quad (5b)$$

$$H_{EM} = \sum_{p,k_z} \hbar \omega_{p,(\vec{q},k_z)} c_{p,(\vec{q},k_z)}^\dagger c_{p,(\vec{q},k_z)}, \quad (5c)$$

$$H_i = \sum_{j,n,p,k_z} i\hbar g_{j,n,p} B_{j,\vec{q}+G_{\parallel}^n}^\dagger c_{p,(\vec{q},k_z)} + \text{H.c.}, \quad (5d)$$

where

$$g_{j,n,p} = - \frac{\varepsilon_{j,\vec{q}+G_{\parallel}^n}}{\hbar \sqrt{2\hbar \omega_{p,(\vec{q},k_z)}} \epsilon_0 l} \phi(0) d_j u_{j,n,p}. \quad (5e)$$

Here,  $B_{j,\vec{q}}^\dagger$  ( $B_{j,\vec{q}}$ ) creates (annihilates) an exciton with the ‘‘bare’’ dispersion  $\varepsilon_{j,\vec{q}}$  (due to electronic hopping alone). The index  $j$  ( $\equiv$  T, L, Z) denotes the exciton polarization, as described in Sec. II B and the Appendix.  $c_{p,(\vec{q},k_z)}^\dagger$  ( $c_{p,(\vec{q},k_z)}$ ) creates (annihilates) a 3D Bloch mode photon in photonic band  $p$ , with wave vector  $(\vec{q}, k_z)$  with frequency  $\omega_{p,(\vec{q},k_z)}$ . From Eq. (5e), we see that the coupling  $g_{j,n,p}$  of the  $j$ -polarized exciton of wave vector  $\vec{q}+G_{\parallel}^n$  to photons in band  $p$  is proportional to  $d_j$ , the magnitude of the  $j$ -exciton dipole, and  $u_{j,n,p}$ , the Fourier component  $\vec{q}+G_{\parallel}^n$  of the electric field in the  $j$  direction. To perform numerical calculation, we also assume the following exciton parameters.  $\phi(0)=1.6 \times 10^8 \text{ m}^{-1}$  is the overlap amplitude in the electron and hole relative movement wave functions, assuming an exciton Bohr radius  $a_B=10 \text{ nm}$ .  $d_j=10^{-28} \text{ C m}$  is the magnitude of the all different polarized exciton dipole. The parameter  $l$  is the sample (quantization) length along the  $z$  direction for discretizing the electromagnetic modes.  $l$  is canceled out after performing integration over  $k_z$  for the final exciton renormalization.  $\epsilon_0$  is the permittivity of free space. Since we consider exciton nearly resonant with a photonic band edge appearing at a certain wave vector position, we attribute the field pattern at the band edge for the band  $p$  to the entire band  $p$  in approximating the coupling parameters  $\{u_{j,n,p}\}$ . Variations of these couplings at far away, off-resonant wave vectors make negligible change to the final dressed exciton energies.

The model Hamiltonian [Eqs. (5)] of QW exciton in the engineered PBG vacuum is parametrized by the quasimomentum  $\vec{q}$ , which is a constant of motion for the exciton. Consequently, the model [Eqs. (5)] represents (one of) a family of Hamiltonians spanning the various conserved exciton momenta. In what follows, we demonstrate that when the exciton wave vector approaches one of the photonic band edges, a dramatic renormalization of exciton properties takes place.

Before proceeding to a detailed evaluation of exciton dressing by photonic crystal modes, we consider a simplified model to illustrate the coherent radiative hopping process resulting from interaction with light. From photonic band structure calculations, it is straightforward to verify that the photon effective mass is typically 5 orders of magnitude smaller than the exciton effective mass at the relevant photonic band edges. Therefore, it is instructive to first neglect the exciton dispersion (set the bare exciton effective mass to infinity) and replace  $\varepsilon_{j,\vec{q}+G_{\parallel}^n}$  by a wave vector independent constant  $\varepsilon_b$  in Eqs. (5b) and (5e). We simplify the model to

treat only one photonic band edge interacting with the exciton (see also Sec. III B), and we also neglect the photon dispersion in the coupling constant near resonance. The simplified Hamiltonian becomes

$$H = H_0 + H_i, \quad (6a)$$

$$H_0 = \varepsilon_b D_{\vec{q}}^\dagger D_{\vec{q}} + \sum_{k_z} \hbar \omega_{(\vec{q},k_z)} c_{\vec{q},k_z}^\dagger c_{\vec{q},k_z}, \quad (6b)$$

$$H_i = \sum_{k_z} i\hbar \tilde{g} D_{\vec{q}}^\dagger c_{\vec{q},k_z} + \text{H.c.} \quad (6c)$$

We show in Sec. III A that the coupling constant  $\tilde{g}$  and the new form of exciton creation operator  $D_{\vec{q}}^\dagger$  for this simplified Hamiltonian can be related to those of the original Hamiltonian in Eqs. (5) by the relations

$$\tilde{g} = \sqrt{\sum_{j,n} g_{j,n} g_{j,n}^*}, \quad (6d)$$

$$D_{\vec{q}}^\dagger = \sum_{j,n} \frac{g_{j,n}}{\tilde{g}} B_{j,\vec{q}+G_{\parallel}^n}^\dagger. \quad (6e)$$

Given the discrete translational symmetry in the QW plane and the broken translational symmetry normal to the QW plane, the in-plane wave vector  $q$  is conserved and the out-of-plane wave vector  $k_z$  can be freely chosen in the first Brillouin zone.

Substituting the coupling term [Eq. (5e)] into Eq. (6d), we obtain  $\tilde{g} = \frac{\omega_0}{\sqrt{2\hbar \epsilon_0 l}} \phi(0) d(\sum u_{j,n} u_{j,n}^*)^{1/2}$  on the condition of exciton-photon resonance and neglecting exciton and photon dispersion in coupling Eq. (5e) ( $\hbar \omega_0 = \varepsilon_{j,\vec{q}+G_{\parallel}^n} = \hbar \omega_{(\vec{q},k_z)}$ ).

To derive the renormalized exciton dispersion mediated by coherent emission and reabsorption of virtual photons, we use the canonical transformation method. A more general variational wave function approach in obtaining the dressed exciton is presented in subsequent sections. Using a unitary transformation  $e^S$ , the original Hamiltonian  $H$  is transformed into the effective Hamiltonian  $H'$  that incorporates radiative dressing into the exciton kinetic energy,

$$\begin{aligned} H' &= e^{-S} H e^S = \sum_{n=0}^{\infty} \frac{1}{n!} [\cdots [[H, S], S] \cdots, S] \\ &= H + [H, S] + \frac{1}{2!} [[H, S], S] + \cdots, \end{aligned} \quad (7a)$$

where

$$S = -F \sum_{k_z} i\hbar \tilde{g} (D_{\vec{q}}^\dagger c_{\vec{q},k_z} + D_{\vec{q}} c_{\vec{q},k_z}^\dagger). \quad (7b)$$

In Eq. (7b), the undetermined parameter  $F$  is chosen to satisfy  $H_i + [H_0, S] = 0$ . This condition eliminates the linear exciton-photon interaction in  $H'$ . This type of transformation has been used in a different physical context, namely, for an interacting many-electron system coupled to phonons. In such a system, the linear electron-phonon coupling is eliminated to obtain a phonon-mediated effective electron-electron interaction relevant to the phenomena of Cooper

pairing and superconductivity.<sup>34</sup> In our exciton-photon model [Eqs. (6)], the linear exciton-photon interaction is eliminated by the choice  $F = (\varepsilon_b - \hbar\omega_{(\vec{q},k_z)})^{-1}$ . In order to extract the effective exciton hopping Hamiltonian  $H_{eff}$  from  $H'$ , we consider all terms that are quadratic in the exciton operators and contain no photon operators. These include  $H_0$  and terms from  $[H_i, S]$ . We obtain the renormalized exciton kinetic energy:

$$H_{eff} = \left( \varepsilon_b + \sum_{k_z} \frac{\hbar^2 \bar{g}^2}{\varepsilon_b - \hbar\omega_{\vec{q},k_z}} \right) D_{\vec{q}}^\dagger D_{\vec{q}}. \quad (8)$$

The revised exciton energy given in brackets in Eq. (8) incorporates the effect of emitting and reabsorbing nonresonant virtual photons of energy  $\hbar\omega_{(\vec{q},k_z)}$ .

When the exciton energy is very near in resonance with the photonic band edge, a more accurate expression for the dressed state energy is required. In what follows, we show that a more precise variational estimate for the exciton energy is obtained by replacing the term  $\varepsilon_b$  in the denominator of [Eq. (8)] by the renormalized energy  $E$  itself. The modification is equivalent to the change from Rayleigh-Schrödinger perturbation theory to Brillouin-Wigner perturbation theory.<sup>35</sup> As we show in Secs. III A and III B, the exciton energy  $E$  is obtained by solving the implicit equation

$$E = \varepsilon_b + \sum_{k_z} \frac{\hbar^2 \bar{g}^2}{E - \hbar\omega_{\vec{q},k_z}}. \quad (9)$$

Substituting the corresponding dispersion of the photonic band edge and performing the integral over  $k_z$ , we will obtain the renormalized exciton dispersion. Equipped with this general understanding about the exciton in this engineered vacuum, we proceed to a more detailed treatment of the specific interactions described by the original model Hamiltonian of Eqs. (5).

### A. Exciton interaction with planar guided band edge

Planar guided modes appearing in the PBG due to the QW defect layer are evanescent in the normal direction but freely propagate along the QW. Our numerical calculation reveals that only the lowest planar guided mode is strongly polarized both in plane and perpendicular to the band-edge wave vector  $\vec{q}$ . This band-edge mode couples strongly to the T exciton. In the absence of nearby 3D extended modes, we can eliminate the sum over  $k_z$  in the general Hamiltonian shown in Eqs. (5). The reduced Hamiltonian for a T exciton coupled to the lowest planar guided electromagnetic mode is

$$H = H_{exc} + H_{EM} + H_i, \quad (10a)$$

$$H_{exc} = \sum_n \varepsilon_{\vec{q}+G_{\parallel}^n} B_{\vec{q}+G_{\parallel}^n}^\dagger B_{\vec{q}+G_{\parallel}^n}, \quad (10b)$$

$$H_{EM} = \hbar\omega_{\vec{q}} c_{\vec{q}}^\dagger c_{\vec{q}}, \quad (10c)$$

$$H_i = \sum_n i\hbar g_n B_{\vec{q}+G_{\parallel}^n}^\dagger c_{\vec{q}} + \text{H.c.}, \quad (10d)$$

$$g_n = - \sqrt{\frac{\omega_0}{2\hbar\varepsilon_0}} \phi(\rho=0) du_{G_{\parallel}^n}. \quad (10e)$$

Here,  $\omega_0$  represents both the exciton recombination energy and the planar guided band-edge photon energy, since they are nearly in resonance. We neglect the photon and exciton dispersion in obtaining the coupling constants in Eq. (10e). All other notations are the same as in Eqs. (5). The reduced model [Eq. (10)] represents a continuous one-parameter family of Hamiltonians for each choice of the conserved wave-vector  $\vec{q}$ .

In the following, we provide a more precise variational approach to obtain the dressed exciton dispersion without recourse to the canonical transformation method described above. From the interaction Hamiltonian [Eq. (10d)], we observe that the planar guided photon of wave vector  $\vec{q}$  only couples to an exciton of wave vector  $\vec{q} + G_{\parallel}^n$ , where  $\{G_{\parallel}^n\}$  is the set of in-plane photonic crystal reciprocal lattice vectors. The dressed exciton eigenstate must then be the linear superposition of the corresponding exciton states and the planar guided photon. This can be expressed using a variational wave function in the Schrödinger picture:

$$|\vec{q}\rangle_{dressed}^{exc} = \sum_n b_{G_{\parallel}^n} |\vec{q} + G_{\parallel}^n\rangle_{bare}^{exc} + b_{photon}^{2D} |\vec{q}\rangle_{photon}^{2D}, \quad (11)$$

Here,  $|\vec{q} + G_{\parallel}^n\rangle_{bare}^{exc}$  represents a single bare exciton of wave vector  $\vec{q} + G_{\parallel}^n$  and zero photons.  $|\vec{q}\rangle_{photon}^{2D}$  represent a single 2D photon in the planar guided photonic mode and no exciton present.  $b_{G_{\parallel}^n}$  and  $b_{photon}^{2D}$  are variational amplitudes of bare exciton eigenstates and the planar guided photon, respectively. This variational ansatz for the dressed exciton at wave vector  $\vec{q}$ , denoted by  $|\vec{q}\rangle_{dressed}^{exc}$ , considers only contributions from the single exciton and single-photon sectors of the many-electron, multiphoton Hilbert space. Within this subspace of the larger Hilbert space, the Schrödinger equation for the dressed exciton becomes

$$\begin{pmatrix} \varepsilon_{\vec{q}+G_{\parallel}^1} & 0 & \cdots & 0 & i\hbar g_1 \\ 0 & \varepsilon_{\vec{q}+G_{\parallel}^2} & \cdots & 0 & i\hbar g_2 \\ \vdots & \vdots & \ddots & 0 & \vdots \\ 0 & 0 & \cdots & \varepsilon_{\vec{q}+G_{\parallel}^n} & i\hbar g_n \\ -i\hbar g_1^* & -i\hbar g_2^* & \cdots & -i\hbar g_n^* & \hbar\omega_{\vec{q}} \end{pmatrix} \begin{pmatrix} b_{G_{\parallel}^1} \\ b_{G_{\parallel}^2} \\ \vdots \\ b_{G_{\parallel}^n} \\ b_{photon}^{2D} \end{pmatrix} = E \begin{pmatrix} b_{G_{\parallel}^1} \\ b_{G_{\parallel}^2} \\ \vdots \\ b_{G_{\parallel}^n} \\ b_{photon}^{2D} \end{pmatrix}. \quad (12)$$

Here, the energy eigenvalue  $E$  for the dressed exciton implicitly depends on the conserved crystal momentum parameter  $q$ , and this defines the dressed exciton dispersion relation as it is renormalized by the radiative (virtual photon) hopping process. From Eq. (12), it is straightforward to derive the following eigenvalue condition:

$$\sum_n \frac{\hbar^2 g_n g_n^*}{(\varepsilon_{\vec{q}+G_{\parallel}^n} - E)(\hbar\omega_{\vec{q}} - E)} = 1. \quad (13)$$

After solving Eq. (13) for the eigenenergy  $E$ , it follows that the variational amplitudes satisfy the condition

$$b_{G_{\parallel}^n} = b_{\text{photon}}^{2D} \frac{\hbar g_n^*}{\varepsilon_{\vec{q}+G_{\parallel}^n} - E}. \quad (14)$$

$b_{\text{photon}}^{2D}$  is, in turn, obtained by the normalization of the dressed exciton eigenstate [Eq. (11)].

As in the illustration provided by the simplified model Hamiltonian [Eq. (6)], it is instructive to consider the limit in which bare exciton has an infinite effective mass. In this case, the bare exciton is dispersionless and we may set  $\varepsilon_{q+G_{\parallel}} = \varepsilon_b$ , the wave vector independent electron-hole recombination energy. As it turns out (for realistic exciton parameters), the bare exciton dispersion makes relatively small contribution (compared with coherent radiative hopping) to the dressed exciton dispersion relation. In the exciton infinite effective-mass approximation, Eq. (13) is reduced to

$$(\varepsilon_b - E)(\hbar\omega_{\vec{q}} - E) - \hbar^2 \tilde{g}^2 = 0, \quad (15a)$$

where the effective coupling constant is defined as  $\tilde{g} = (\sum_n g_n g_n^*)^{1/2}$ . The resulting two dispersion branches are given by

$$E = \frac{\varepsilon_b + \hbar\omega_{\vec{q}} \pm \sqrt{(\varepsilon_b - \hbar\omega_{\vec{q}})^2 + 4\hbar^2 \tilde{g}^2}}{2}. \quad (15b)$$

The energy difference between these two branches is the excitonic equivalent of vacuum Rabi splitting.<sup>4-6</sup> The original interaction Hamiltonian [Eq. (10d)] can be rewritten using the infinite effective-mass coupling constant as

$$H_i = i\hbar\tilde{g}D_{\vec{q}}^{\dagger}c_{\vec{q}} + \text{H.c.}, \quad (16)$$

where we have defined the modified exciton creation operator

$$D_{\vec{q}}^{\dagger} = \sum_n \frac{g_n}{\tilde{g}} B_{\vec{q}+G_{\parallel}^n}^{\dagger}. \quad (17)$$

If we now assume that  $\varepsilon_{q+G_{\parallel}} = \varepsilon_b$  (infinite effective mass), the Hamiltonian [Eq. (10)] reduces to

$$\tilde{H} = \varepsilon_b D_{\vec{q}}^{\dagger} D_{\vec{q}} + \hbar\omega_{\vec{q}} c_{\vec{q}}^{\dagger} c_{\vec{q}} + i\hbar\tilde{g}(D_{\vec{q}}^{\dagger} c_{\vec{q}} - c_{\vec{q}}^{\dagger} D_{\vec{q}}). \quad (18)$$

Diagonalizing  $\tilde{H}$  reproduces the eigenvalue solutions [Eq. (15b)].

If we include the bare exciton dispersion in the evaluation of the dressed state energies, we must truncate the matrix Schrödinger equation [Eq. (12)] at a certain  $G_{\parallel}^n$  and solve it numerically. In this case, we consider only the T exciton in our model Hamiltonian. To obtain the coupling coefficient, we require the transverse part of the Fourier component  $\vec{u}(\vec{\rho}, z_0)$  of the electric field in Eq. (2), where  $z_0$  is the position of QW in the PBG-QW heterostructure. This leads to a

numerically tractable matrix equation since the main contribution of the electromagnetic field comes from lower orders of  $G_{\parallel}^n$ .

For concreteness, we consider a heterostructure consisting of a QW sandwiched by woodpile<sup>27</sup> PBG material [see Figs. 1(a) and 1(b)]. The woodpile structure consists of rod stacks with rectangular cross section. The width and height of the rods are  $0.25a$  and  $0.3a$ , respectively, where  $a$  is the lattice constant (the distance between two adjacent rods in the same layer). One unit cell of woodpile consists of four stacking layers. Therefore, the vertical periodicity in the stacking direction is  $1.2a$ . The QW thickness is chosen to be  $0.06a$ . Using a dielectric constant of 11.9 for both the PBG material and the QW, the lowest 2D planar guided band edge [red line in Fig. 1(b)] appears at frequency of  $0.400 \frac{2\pi c}{a}$ . We assume that the exciton binding energy is 0.8266 eV, corresponding to a recombinative radiative emission at wavelength of  $1.5 \mu\text{m}$ . If the exciton is in resonance with the 2D photonic band edge, the lattice constant is 600 nm. Recently, Noda *et al.*<sup>28</sup> have fabricated a flat light-emitting layer composed of three InGaAsP multiple quantum wells with emission wavelength around  $1.5 \mu\text{m}$  sandwiched above and below by one unit cell of the GaAs 3D woodpile structure. In our design, we sandwich the MQW by more unit cells of woodpile structure and extend this thin light-emitting layer over a larger area so that the exciton wave vector is a good quantum number. Nevertheless, the experimentally fabricated architecture<sup>28,32</sup> clearly points to the materials suitable for our design and indicates the feasibility of our PBG-QW heterostructure.

From the eigenvalue equation [Eq. (13)], we can see that anisotropic photonic dispersion leads to anisotropic renormalized exciton dispersion. After diagonalizing the matrix [Eq. (12)] in the case of dispersionless exciton, we obtain two new eigenstates that we refer to as the upper and lower exciton-polaritons. Using the numerically calculated planar guided mode by FDTD together with the assumption of exciton Bohr radius  $a_B = 10 \text{ nm}$  [ $\phi(0) = 1.59 \times 10^8 \text{ m}^{-1}$ ], exciton recombination energy of 0.8266 eV, and dipole moment  $d = 10^{-28} \text{ C m}$ , we obtain the effective coupling  $\hbar\tilde{g} = 8.2 \text{ meV}$  and then the normal mode splitting of about 16 meV. A similar description has been used<sup>36</sup> for coupled exciton-photon mode splitting in a semiconductor microcavity. Here, we stress some major differences between the conventional cavity exciton-polariton and our exciton-photon bound state. In Ref. 36, the cavity photon mode distributes uniformly on the QW plane and the dressed exciton ground state is centered at the  $\Gamma$  point (wavevector is  $[0, 0]$ ). In order to reduce coupling to the continuum of photon states at the interface with air, a large stack ( $\sim 57$ ) of quarter-wave semiconductor layers<sup>36</sup> is required. The exciton can nevertheless decay by coupling to photons (propagating off normal to the Bragg stack) that are outside the 1D stop gap of the cavity mirrors. Our PBG photons reside in fundamentally “guided” modes (centered at high symmetry wave vector points), which are decoupled from the photon continuum states at the sample boundaries above and below the QW. There is no decay of the exciton due to coupling to nonguided modes. The exciton-planar guided photon splitting in our paper is analogous to the idealized exciton-polariton in 3D bulk semi-

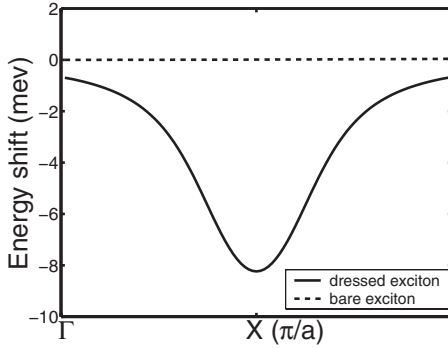


FIG. 3. Renormalized exciton dispersion for the model of a dispersionless bare exciton (infinite effective mass) resonantly interacting with the 2D planar guided photonic band in woodpile QW heterostructure. The solid line shows the dispersion of the lower dressed exciton-polariton state. For comparison, the dashed line shows the original exciton dispersion with effective mass of  $0.1m_e$ . The ground state shifts from  $\Gamma$  ( $\vec{q}=0$ ) to the 2D planar guided band edge at  $X$ . Here,  $a$  is the photonic crystal lattice constant, and the  $y$  axis shows the shifted energy relative to the bare exciton recombination energy.

conductor described by Hopfield.<sup>12</sup> Here the exciton and photon both have well-defined energy and wave vector. Irreversible exciton decay occurs only through scattering of polaritons by other material excitations such as phonons. In practice, photon confinement by Bragg mirrors<sup>36</sup> is weak, and it is necessary to increase the number of QWs to effectively increase the exciton-photon coupling in order to observe this coupled exciton-photon mode splitting. Our 3D PBG architecture provides much stronger confinement of the cavity photon leading to strong interaction with exciton. Our numerical results show that the mode splitting is in the range 10–16 meV (double the energy depth of the local dispersion minimum) for a single QW in the PBG material.

We now focus on the lower exciton-polariton which determines the ground state of the dressed exciton in our 3D PBG architecture. Firstly, comparing the band structure calculation shown in Fig. 1(b) and the planar guided photon dispersion model ( $i=1$ ) in Eq. (1), we obtain  $(A_x^{(1)}, A_y^{(1)}) = (0.52, 0.8)$  and  $(q_x, q_y) = (0.5, 0)\frac{2\pi}{a}$ , and then substituting these parameters together with others described, we obtain the following numerical figures. Figure 3 shows the dispersion of the dressed exciton along the  $x$  axis for a dispersionless bare exciton resonantly interacting with the 2D planar guided band-edge photons. Remarkably, this photon interaction creates a deep local minimum in the dressed exciton dispersion relation near the 2D photonic band-edge wave vector. The dressed exciton lowers its energy considerably through coherent radiative hopping by emission and reabsorption of band-edge photons. The relative insensitivity of the renormalized exciton ground state energy to the bare exciton effective mass is shown in Fig. 4. For a broad range (shown on a logarithmic scale) of bare exciton effective masses (electronic dispersion), the depth of the exciton-polariton dispersion remains over 8 meV. For a bare exciton effective mass of  $1m_e$ , the renormalized dispersion depth is almost the same as for an infinite effective-mass exciton in-

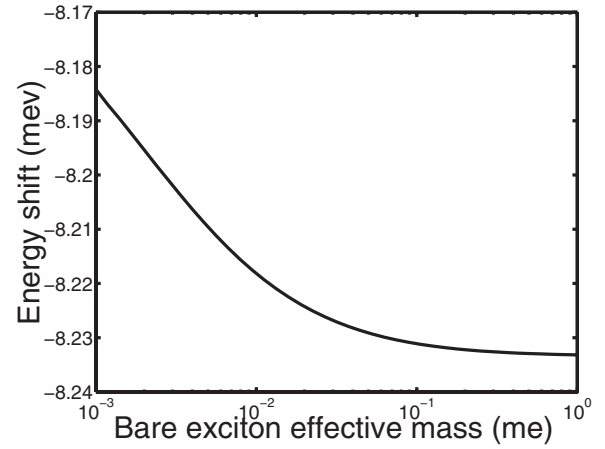


FIG. 4. Dressed exciton energy shift for the model of exciton resonantly interacting with 2D planar guided photonic band of woodpile QW heterostructure. The solid line shows shifted energy (relative to the bare exciton recombination energy) of the local minimum in the dressed exciton-polariton dispersion as a function of the bare exciton effective mass. The typical values for bare exciton effective mass in semiconductor are between  $1m_e$  and  $0.01m_e$  ( $m_e$  is the electron mass). In this range, the bare exciton dynamics has negligible influence on the dressed exciton ground state.

teracting with the planar guided photon. For bare exciton mass between  $0.1m_e$  and  $0.01m_e$  (the typical values for semiconductors), the depth does not change very much. Even if the exciton effective mass is chosen artificially small, the dispersion is still about 5 meV. This insensitivity arises from the separation of length scales between the electronic lattice constant and the photonic crystal lattice constant. The relevant photonic Bloch modes are dominated by Fourier components of wave vector much smaller than the typical wave vectors for bare exciton motion. The change in bare exciton energy on the scale of the photon wave vector is very small, and the exciton remains in resonance with the photonic band edge over this range of energies. This justifies our neglect of exciton dispersion in the simplified models [Eqs. (6) and (18)] for the case of exciton in close resonance with the photonic band edge.

The magnitude of the dressed exciton local minimum as a function of the detuning ( $\epsilon_b - \hbar\omega_{2D}$ ) between the bare exciton binding energy and the 2D photonic band-edge frequency is shown in Fig. 5. The maximum amplitude is about 8.2 meV at zero detuning. This suggests that the exciton capture by this 2D band edge could survive thermal fluctuations of roughly 80 K. This depth decreases with increasing detuning. Figure 6 shows the effective mass of the lower exciton-polariton captured near the photonic band edge as a function of the detuning. Clearly, the effective mass remains about 4 orders of magnitude less than the electron mass over a significant range of detuning of the bare exciton from the 2D band edge. The resulting dressed exciton exhibits very high mobility. On resonance, the dressed exciton effective mass is about half of that of the planar guided photon, in agreement with the analytical result obtained from Eq. (15b). In Fig. 6, we assume that the coupling constants in Eq. (10e) are independent of the quasi-wave-vector  $\vec{q}$ , since we focus on the region near the band-edge wave vector.

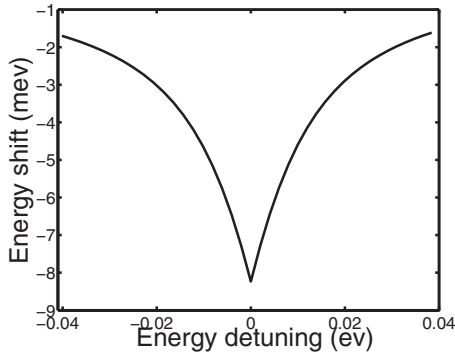


FIG. 5. For the model of dispersionless exciton interacting with 2D planar band edge in woodpile QW heterostructure, solid line shows the magnitude of the dressed exciton local minimum as a function of the detuning ( $\varepsilon_b - \hbar\omega_{2D}$ ) between the bare exciton binding energy and the 2D photonic band-edge frequency.

We now consider the realistic dispersion of the planar guided photon in the first Brillouin zone (instead of band-edge effective-mass approximation) to obtain the quantitative dispersion relation of the lower dressed exciton. In order to perform the numerical calculation, we create a grid of discrete points in the first Brillouin, each point on the mesh representing a different wave vector  $\vec{q}$ . In principle, we can calculate the electric field distribution and 2D guided mode frequency for each  $\vec{q}$  by FDTD method. Given the field distribution, we can construct the Hamiltonian matrix [Eq. (12)] and diagonalize the matrix to obtain the lower dressed exciton energy at each wave vector  $\vec{q}$  in the first Brillouin zone. In practice, we approximate the electric field distribution for all  $\vec{q}$  as being that of the band-edge field distribution. Then, only the detuning between the exciton recombination energy and the 2D photon band-edge frequency  $\omega_1$  appears explicitly in the matrix [Eq. (12)]. Using this approximate description, the dispersion of the dressed exciton is calculated as shown in Fig. 7 on resonance (zero detuning). Figure 8 shows the original dispersion of the 2D guided photon band. There are four band edges appearing at high symmetry points,  $\vec{q}=[0.5,0],[0,0.5],[-0.5,0],[0,-0.5]$ . When the bare exciton energy nearly coincides with the 2D band-edge photon, the dressed exciton ground state energy (at high

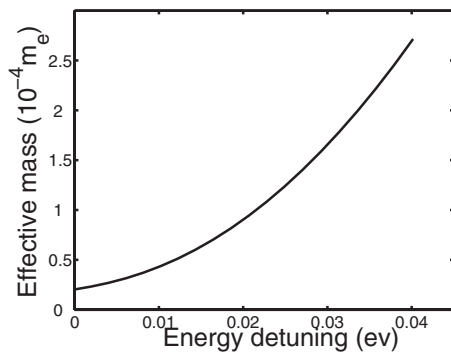


FIG. 6. For the model of dispersionless exciton interacting with 2D planar guided band edge in woodpile QW heterostructure, the solid line shows the effective mass (in units of  $10^{-4}m_e$ ) of the lower exciton-polariton along the  $x$  direction captured at  $\vec{q}=[0.5,0]^{\frac{2\pi}{a}}$ .

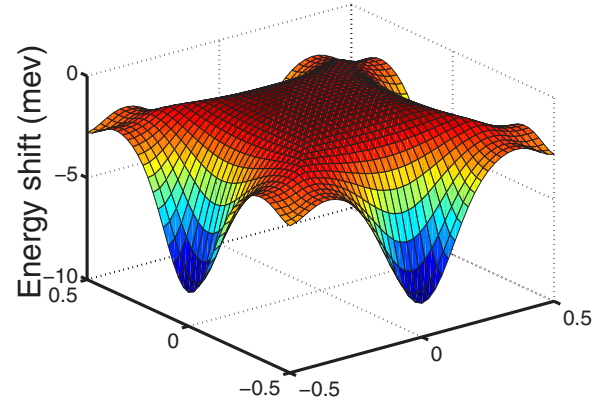


FIG. 7. (Color online) For the model of dispersionless exciton resonantly interacting with the 2D planar guided band in woodpile QW heterostructure, the shaded surface shows the dispersion (energy vs wave vector  $q$ ) of the dressed exciton-polariton in the first Brillouin zone. The dressed exciton ground state appears at high symmetry photonic band-edge wave vector points  $\vec{q}=[0.5,0],[0,0.5],[-0.5,0],[0,-0.5]$  in units of  $\frac{2\pi}{a}$ .

symmetry band-edge wave vector points) is considerably lower than the bare exciton ground state energy at  $\vec{q}=[0,0]$ . As shown in Eq. (11), this dressed exciton of wave vector  $\vec{q}$  is a linear superposition of excitons with wave vectors  $\vec{q} + \vec{G}_\Pi^n$  and the 2D guided photon with wave vector  $\vec{q}$ .

From the modified infinite effective-mass exciton creation operator [Eq. (17)], we observe that the envelope of the exciton component of the dressed ground state mirrors the electric field of the corresponding photonic band edge. In our current exciton-2D planar photon interaction model, only the T exciton is considered. In this case, the amplitude of electric field perpendicular to the wave vector  $\vec{q}$  closely resembles the exciton envelope wave function. This is depicted in Fig. 9(a), where the square of the electric field amplitude can be interpreted as the exciton probability density in one unit cell on the QW plane. The relative direction between two arrows at two different points shows the relative phase of the electric field of those two points. Figure 9(a) exhibits a nodal (zero

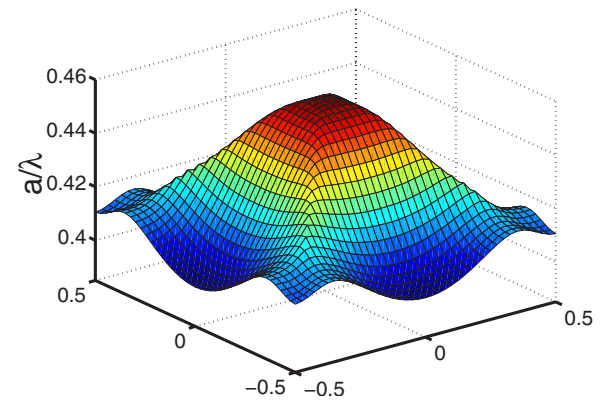


FIG. 8. (Color online) The photonic dispersion surface (energy vs wave vector  $q$ ) of the 2D planar guided band in woodpile QW heterostructure in the first Brillouin zone. There are four minimum frequency band edges at  $\vec{q}=[0.5,0],[0,0.5],[-0.5,0],[0,-0.5]$  in units of  $\frac{2\pi}{a}$ .

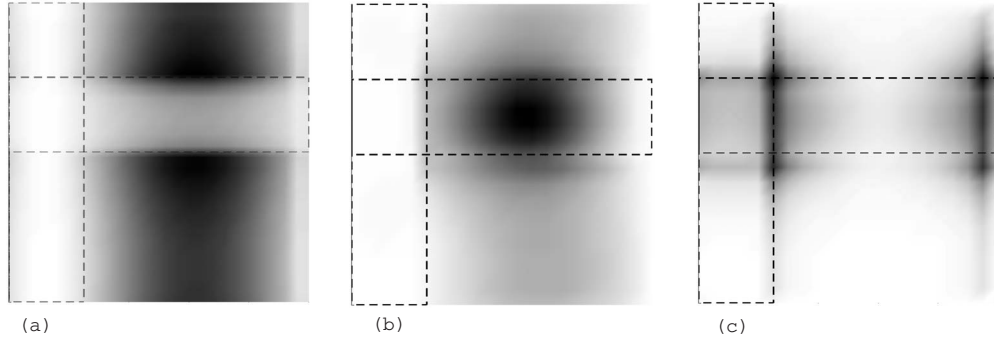


FIG. 9. (a) For the model of a dispersionless exciton resonantly interacting with 2D planar guided band edge in woodpile QW heterostructure, the shading depicts the intensity distribution of the  $y$  component of the planar guided electric field  $[|E_y(x, y, z_o)|^2]$  on the QW plane at position  $z_o$ . The deep dark region indicates the maximum intensity and the light gray region shows the minimum intensity. The loops circled by dashed lines indicate the woodpile rods above and below the QW. For comparison, we show the electric field intensity distribution at the same QW position for the 3D upper band edge at  $q=(0.5, 0, 0.417)\frac{2\pi}{a}$  in (b) and 3D lower band edge at  $q=(0.3, 0, 0)\frac{2\pi}{a}$  in (c).

amplitude) line, suggesting a standing mode electric field distribution on the QW. For realistic bare exciton dispersion, the exciton probability distribution is smoother than that shown in Fig. 9(a). If T and L excitons are both included in our model Hamiltonian [Eq. (10)], the local minimum in the dressed exciton dispersion is slightly (about 10%) deeper than before.

### B. Exciton capture by 3D photonic band edges

In this section, we generalize the variational method used in Sec. III A to solve the Hamiltonian [Eqs. (5)]. This provides a more general eigenvalue equation describing an exciton interacting with more than one photonic band edge.

From the interaction Hamiltonian [Eq. (5d)], we observe that excitons with different wave vectors  $\vec{q} + G_{\parallel}^n$  are indirectly coupled through the process of emitting and reabsorbing virtual Bloch mode photons with band label  $p$  and wave vector  $(q, k_z)$ , where  $k_z$  can be freely chosen. Now, the dressed exciton eigenstate is a more complicated linear superposition of bare exciton states and photonic Bloch modes. This can again be expressed as a variational wave function in the Schrödinger picture:

$$|\vec{q}\rangle_{dressed}^{exc} = \sum_{j,n} b_{j,n}^{exc} |j, \vec{q} + G_{\parallel}^n\rangle_{bare}^{exc} + \sum_{p,k_z} b_{p,(\vec{q},k_z)}^{photon} |p, (\vec{q}, k_z)\rangle^{photon}. \quad (19a)$$

Here,  $|j, \vec{q} + G_{\parallel}^n\rangle_{bare}^{exc}$  represents a single bare  $j \equiv (T, L, Z)$  exciton of wave vector  $\vec{q} + G_{\parallel}^n$  and zero photons.  $|p, (\vec{q}, k_z)\rangle^{photon}$  represents a single 3D photon in band  $p$  with wave vector  $(\vec{q}, k_z)$  and no exciton.  $b_{j,n}$  and  $b_{p,(\vec{q},k_z)}^{photon}$  are variational amplitudes of bare exciton eigenstates and the 3D photons, respectively. This variational ansatz for the dressed exciton at wave vector  $\vec{q}$ , denoted by  $|\vec{q}\rangle_{dressed}^{exc}$ , considers only contributions from the single exciton and single-photon sectors of the many-electron, multiphoton Hilbert space and  $E$  is the corresponding eigenenergy.

The corresponding Schrödinger equation is

$$H|\vec{q}\rangle_{dressed}^{exc} = E|\vec{q}\rangle_{dressed}^{exc}. \quad (19b)$$

Projecting Eq. (19b) into the space spanned by the states  $|j, \vec{q} + G_{\parallel}^n\rangle_{bare}^{exc}$  and  $|p, (\vec{q}, k_z)\rangle^{photon}$ , we obtain the following equations:

$$\varepsilon_{j,\vec{q}+G_{\parallel}^n} b_{j,n}^{exc} + i\hbar \sum_{p,k_z} g_{j,n,p} b_{p,(\vec{q},k_z)}^{photon} = E b_{j,n}^{exc}, \quad (20a)$$

$$\hbar\omega_{p,(\vec{q},k_z)} b_{p,(\vec{q},k_z)}^{photon} - i\hbar \sum_{j,n} g_{j,n,p}^* b_{j,n}^{exc} = E b_{p,(\vec{q},k_z)}^{photon}. \quad (20b)$$

From Eqs. (20a) and (20b), we obtain

$$b_{j,n}^{exc} = \frac{i\hbar \sum_{p} g_{j,n,p} A_p}{E - \varepsilon_{j,\vec{q}+G_{\parallel}^n}}, \quad (21a)$$

$$b_{p,(\vec{q},k_z)}^{photon} = \frac{-i\hbar \sum_{j,n} g_{j,n,p}^* b_{j,n}^{exc}}{E - \hbar\omega_{p,(\vec{q},k_z)}}, \quad (21b)$$

where

$$A_p \equiv \sum_{k_z} b_{p,(\vec{q},k_z)}^{photon}. \quad (21c)$$

Substituting Eq. (21a) into Eq. (21b) and performing the sum over  $k_z$  on both sides of Eq. (21b), we obtain the condition

$$A_p = \sum_{j,n,k_z} \frac{-i\hbar g_{j,n,p}^* \left( i\hbar \sum_{p'} g_{j,n,p'} A_{p'} \right)}{(E - \hbar\omega_{p,(\vec{q},k_z)})(E - \varepsilon_{j,\vec{q}+G_{\parallel}^n})}. \quad (22)$$

In order to evaluate the energy eigenvalue  $E$ , it is useful to rewrite this as

$$\sum_{j,n,k_z} \left( \frac{\hbar^2 g_{j,n,p}^* g_{j,n,p}}{(E - \hbar \omega_{p,(\vec{q},k_z)})(E - \varepsilon_{j,\vec{q}+G_{\parallel}^n})} - 1 \right) A_p + \sum_{p' \neq p, j, n, k_z} \frac{\hbar^2 g_{j,n,p}^* g_{j,n,p'}}{(E - \hbar \omega_{p,(\vec{q},k_z)})(E - \varepsilon_{j,\vec{q}+G_{\parallel}^n})} A_{p'} = 0 \quad (23)$$

Equation (23) consists of  $p$  equations, one for each photonic band. A nontrivial solution of this set of homogeneous, linear equations exists provided that the determinant of the corresponding matrix of coefficients is zero. This yields the required eigenvalue equation. While Eq. (23) is a very general equation for an exciton interacting with multiple photonic bands (different  $p$ ), it is often the case that one photonic band edge interacts dominantly when the exciton recombination energy is in near resonance with that band edge. In this case, the dominant features of the eigenvalue spectrum ( $E$  vs  $\vec{q}$ ) can be reproduced by eliminating all other photonic bands.

Many PBG architectures exhibit nondegenerate photonic band edges as evident from band structure calculation. Some PBG materials (like woodpile) exhibit degeneracy at certain band-edge wave vectors in the infinite crystal idealization. Finite sample size and sample boundary conditions may lift such degeneracy. If the exciton is in near resonance with one photonic band edge, we can typically neglect further removed photonic band edges, since the dressed exciton energy shift decreases with detuning as shown in Figs. 5 and 12.

In typical PBG materials, different photonic band edges have different field polarization contents and intensity maxima at different positions. This is also true for the PBG-QW heterostructure. We consider two upper band Bloch modes at the wave vector  $(0.5, 0, 0.26)\frac{2\pi}{a}$  to illustrate this point. We refer to the 3D upper band-edge mode as band 1, and next higher band as band 2. Detailed electric field distribution calculations (using FDTD) show that these two photonic bands exhibit quite different polarization contents. Band 1 has a relatively strong electric field component in plane along the  $y$  direction, whereas band 2 has a strong electric polarization along the normal  $z$  direction. These mode profiles also vary as the vertical position of the cutting plane (where the QW layer is inserted within the 3D PBG material) is changed. This implies that the exciton-photon coupling varies with the vertical placement of the insertion plane. In order to track this variation, we plot the in-plane electric field integral over the QW plane in one unit cell  $[\int_{QW \text{ plane in one unit cell}} (|\vec{E}_x|^2 + |\vec{E}_y|^2) dx dy]$  as a function of QW insertion position in the  $z$  direction for the two bands in Fig. 10. The dashed line corresponds to band 1 and dotted line corresponds to band 2. The solid line gives the overlap integral of the two in-plane, band-edge electric fields between these two photonic bands. Clearly, the dashed line is much higher than the dotted line and the dashed line is peaked at certain insertion positions. This is indicative of the fact that the in-plane polarization content (relevant to exciton-photon coupling) is larger for band 1 than for band 2. We give the in-plane electric field distribution at the optimal insertion

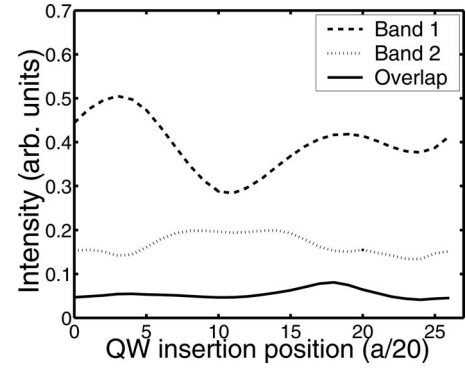


FIG. 10. For the model of a dispersionless exciton resonantly interacting with 3D upper band edge in DSS:1 QW heterostructure, the in-plane electric field integral over the QW plane in one unit cell  $[\int_{QW \text{ plane in one unit cell}} (|\vec{E}_x|^2 + |\vec{E}_y|^2) dx dy]$  is depicted as a function of QW insertion position in the  $z$  direction for band 1 (dashed line) and band 2 (dotted line). The solid line gives the overlap integral of the two in-plane, band-edge electric fields between these two photonic bands.

plane in Fig. 11. In Fig. 11, the shading indicates the in-plane electric field intensity and the arrows provide a snapshot of the in-plane electric field amplitude. The relative arrow directions at different positions represent the relative phase of the in-plane electric field vector. The in-plane electric field is confined to certain spatial positions and specific polarizations. This leads to a small overlap (solid line in Fig. 10) between different photonic bands. More fundamentally, the small overlap between different modes comes from the orthogonality of the different vector fields (including full polarization content). By suitable choice of the QW insertion

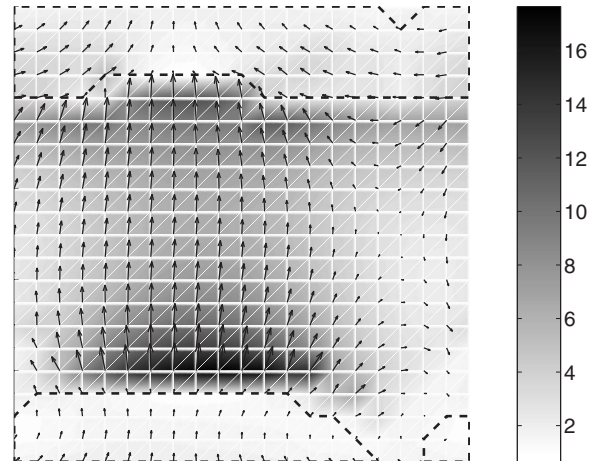


FIG. 11. For the model of a dispersionless exciton resonantly interacting with the 3D upper band edge in DSS:1 QW heterostructure, the shading depicts in-plane electric field intensity distribution at the optical insertion plane  $0.2a$ . Arrows provide a snapshot of the in-plane electric field amplitude. The relative arrow directions at different positions represent the relative phase of the in-plane electric field vector. The in-plane electric field is confined to certain spatial positions (strongest at the deep dark region) with some specific polarizations. The loop circled by dashed lines indicate the dielectric distribution around the QW.

plane, we can enhance the exciton-photon interaction for a specific photonic band edge. If the exciton is captured by this photonic band edge, the wave-field orthogonality condition automatically decreases exciton coupling to other nearby photonic band edges.

The above arguments apply with equal force to the 2D planar guided band edges. As shown in Figs. 1(b) and 2(b), the eigenfrequencies of these modes are far away from the upper or lower 3D band edges. Our numerical calculation shows that the second planar guided band (closer to the 3D upper band edge) interacts very weakly with the T and L exciton in contrast to their strong interaction with the lower planar band edge.

#### IV. EXCITON CAPTURE IN THE EFFECTIVE-MASS APPROXIMATION

In this section, we derive simple analytical approximations for the dressing and capture of excitons by photonic band edges using the effective-mass approximation for photons in the PBG-QW heterostructure. The analysis is also simplified by neglecting the bare kinetic energy of the exciton due to purely electronic hopping motion within the QW. Our numerical results for exciton interaction with the 2D planar guided band confirm that the bare exciton dispersion has a negligible effect on the final dressed exciton dispersion. Likewise, for the 3D photonic band edges, the dressed exciton dispersion is dominated by radiative corrections. Instructive analytical results are obtained by considering a dispersionless ( $\varepsilon_{j,\vec{q}+G_{\parallel}} = \varepsilon_b$ ) bare exciton interacting with only one 3D photonic band edge. In what follows, we also assume that the different polarization states of the exciton (indexed by  $j$ ) lead to the same electron-hole recombination energy  $\varepsilon_b$ . In this case, only the first term in Eq. (23) needs to be retained. We also suppress the photonic band index  $p$ . The resulting eigenvalue equation,

$$\sum_{j,n,k_z} \frac{\hbar^2 g_{j,n}^* g_{j,n}}{(E - \hbar \omega_{\vec{q},k_z})(E - \varepsilon_b)} = 1, \quad (24)$$

is essentially the same as Eq. (9), which we suggested as a variational solution to the simplified model Hamiltonian [Eq. (6)] obtained by the canonical transformation method.

Since we neglect the dependence of  $u_{j,n}$  (the  $j$  component of the  $n$ th Fourier component the electric field vector), on the wave vector ( $\vec{q}, k_z$ ), we can separate the sum over  $k_z$  and the sum over  $(j,n)$  in Eq. (24). The eigenvalue Eq. (24) then becomes

$$\frac{\hbar^2 \tilde{g}^2 J}{E - \varepsilon_b} = 1, \quad (25a)$$

where

$$J = \sum_{k_z} \frac{1}{E - \hbar \omega_{\vec{q},k_z}} \quad (25b)$$

and  $\tilde{g}$  is precisely the effective exciton-photon coupling defined in the Eq. (6d).

Changing the sum into integral and substituting the band-edge effective-mass dispersion [Eq. (1)], we obtain

$$J = \frac{l}{2\pi} \int dk_z \left\{ E - \hbar \left[ \omega_{\vec{q}}^{(i)} + \frac{ac}{2\pi} A_z^{(i)} (k_z - k_i)^2 \right] \right\}^{-1}, \quad (26a)$$

where

$$\omega_{\vec{q}}^{(i)} = \omega_i + \frac{ac}{2\pi} [A_x^{(i)} (q_x - \vec{q}_x^{(i)})^2 + A_y^{(i)} (q_y - \vec{q}_y^{(i)})^2]. \quad (26b)$$

Here,  $i=2$  corresponds to the upper 3D band edge and  $i=3$  corresponds to the lower 3D band edge.

##### A. Exciton resonance with upper 3D photonic band edge

For the exciton in near resonance with 3D upper band edge, we choose  $i=2$  in Eq. (26). After performing integration, Eq. (26a) becomes

$$J = - \left( \frac{l}{2} \right) \left[ (\hbar \omega_{\vec{q}}^{(2)} - E) \frac{ac}{2\pi} A_z^{(2)} \right]^{-1/2}. \quad (27)$$

On the condition of near resonance, i.e.,  $\varepsilon_b \approx \hbar \omega_{\vec{q}}^{(2)}$ , it is convenient to define the complex variable  $z = E - \varepsilon_b$ . The eigenvalue equation then becomes

$$z = - (z_o^{(2)})^{3/2} (-z)^{-1/2}, \quad (28)$$

where  $z_o = \{ l \hbar^2 \tilde{g}^2 / [2 (\frac{ac}{2\pi} A_z^{(2)})^{1/2}] \}^{2/3}$  has the units of energy. The eigenvalue equation [Eq. (28)] has two physical solutions.  $z_1 = -z_o^{(2)}$  corresponds to a stable exciton-photon bound state in the PBG and represents the new ground state of the dressed exciton.  $z_2 = e^{-i\pi/3} z_o^{(2)}$  is a complex solution that describes a decaying exciton state outside the PBG.

From the solution  $z_1$ , we see that the upper band-edge plays a similar role to the planar guided mode band-edge photon. The interaction of the exciton with band-edge photons creates a local minimum in the dispersion of renormalized exciton. The following results are shown for the model of dispersionless exciton interacting 3D upper band edge ( $A_x^{(2)}=0.7$ ,  $A_y^{(2)}=0.1$ , and  $A_z^{(2)}=0.7$ ) in DSS:1 QW heterostructure. Figure 12 shows the depth of the dispersion minimum as a function of the detuning between the upper band edge and the bare exciton. For the upper 3D band edge, the depth of the dispersion minimum at the band-edge wave vector is about 3 meV on resonance. This depth decreases as the detuning increases. Once the exciton falls into this momentum state of minimum energy, it becomes a more stable and mobile entity. The dressed exciton effective mass is shown in Fig. 13 as a function of the detuning of the electron-hole recombination energy from the photonic band edge. This effective mass is roughly 4 orders of magnitude smaller than in the absence of the PBG environment and can reach five orders less in magnitude when near resonance. The dispersion of the 3D upper band edge in the first Brillouin zone is similar to that of the 2D guided photonic band shown in Fig. 8. If we insert the QW at a height of position  $0.2a$  from the bottom of the unit cell, the electric field intensity shown in Fig. 11 closely corresponds to the exciton probability distribution.

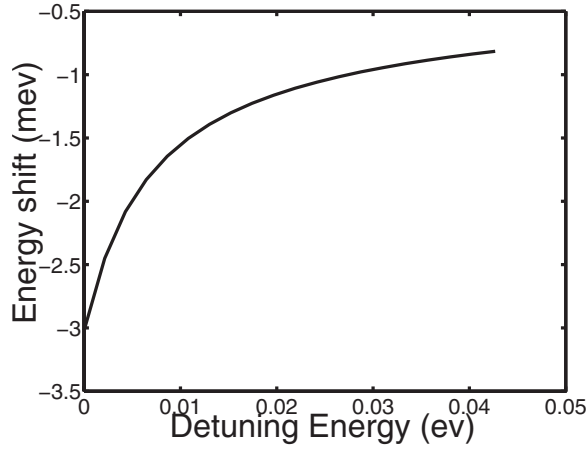


FIG. 12. For the model of a dispersionless exciton interacting with 3D upper band edge in DSS:1 QW heterostructure, solid line shows the magnitude of the dressed exciton local minimum as a function of the detuning below the 3D upper band-edge frequency.

### B. Exciton resonance with lower 3D photonic band edge

For the exciton in resonance with 3D lower photonic band edge, we choose  $i=3$  in Eqs. (26). After performing the integration, we obtain the same result as in Eq. (27) except with the superscript (2) replaced by (3) throughout. On the condition of near resonance, i.e.,  $\varepsilon_b \approx \hbar\omega_{\vec{q}}^{(3)}$ , we substitute the new value of  $J$  into the eigenvalue equation [Eq. (25a)] to obtain

$$z = (z_o^{(3)})^{3/2} z^{-1/2}, \quad (29)$$

where  $z_o^{(3)} = \{l\hbar^2 \tilde{g}^2 / [2(-\frac{ac}{2\pi} A_z^{(3)})^{1/2}]\}^{2/3}$ . As in the case of the upper 3D photonic band edge, there are two physical solutions.  $z_1 = z_o^{(3)}$  corresponds to an exciton-photon bound state in the PBG.  $z_2 = e^{-i2\pi/3} z_o^{(3)}$  is a complex solution that describes a decaying exciton state outside of the PBG.

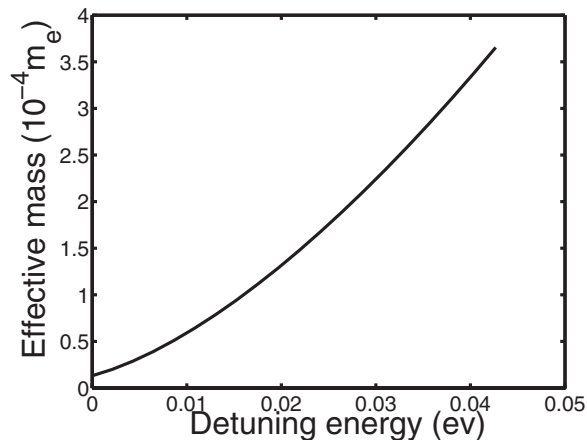


FIG. 13. For the model of dispersionless exciton interacting with 3D upper band edge in DSS:1 QW heterostructure, the solid line shows the renormalized effective mass (in units of  $10^{-4}m_e$ ) of the dressed exciton along the  $x$  direction captured at  $[k_x, k_y] = [0.5, 0] \frac{2\pi}{a}$  as a function of the detuning below the 3D planar band edge.

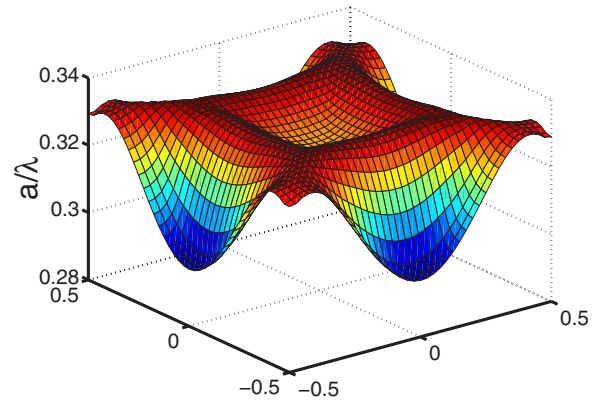


FIG. 14. (Color online) The photonic dispersion surface (energy vs wave vector  $q$ ) of the 3D lower band in DSS:1 QW heterostructure in the first Brillouin zone. The dark ridges (dark red) correspond to the maximum value of the lower band-edge mode. Along these ridges, the photon in-plane effective mass is negative. However, at wave vectors  $\vec{q}=[0,0],[0.5,0],[-0.5,0],[0,0.5],[0,-0.5]$  in units of  $\frac{2\pi}{a}$ , the photon effective mass is positive.

From the solution  $z_1$ , it is apparent that the lower band-edge interaction serves to increase the exciton recombination energy. This is a consequence of the negative photon effective mass along the  $z$  direction. As a result, if we set the exciton in resonance with the negative effective-mass band edge, it is not possible to capture the exciton at the wave vector of this band edge. Figure 14 shows the exact lower band-edge dispersion in the first Brillouin zone. At wave vector positions corresponding to peak values (dark red region) of the lower band-edge mode, the photon in-plane effective mass is negative. However, at wave vectors  $\vec{q}=[0,0],[0.5,0],[-0.5,0],[0,0.5],[0,-0.5]$ , the photon effective mass is positive. Figure 15 shows the renormalized exciton dispersion in the first Brillouin zone when the bare exciton recombination energy is in resonance with the maximum lower band-edge frequency (to obtain this, we take

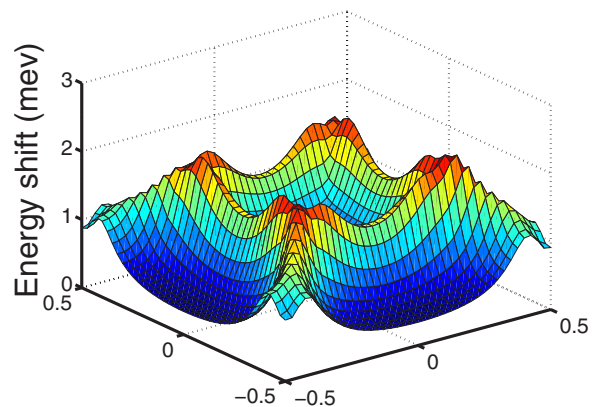


FIG. 15. (Color online) For the model of dispersionless exciton resonantly interacting with 3D lower band edge in DSS:1 QW heterostructure, the shading shows the dispersion (energy vs wave vector  $q$ ) of the renormalized dressed exciton-polariton in the first Brillouin zone. An exciton can be captured with a strongly renormalized small positive effective mass at  $\vec{q}=[0,0],[0.5,0],[-0.5,0],[0,0.5],[0,-0.5]$  in units of  $\frac{2\pi}{a}$ .

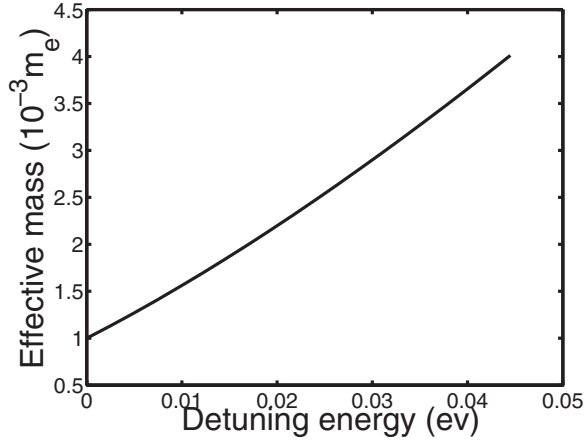


FIG. 16. For the model of dispersionless exciton interacting with 3D lower band edge in DSS:1 QW heterostructure, the solid line shows the effective mass (in units of  $10^{-3}m_e$ ) of the renormalized exciton captured by 3D lower band around the  $\Gamma$  wave vector position as a function of the detuning above the 3D lower edge.

$A_z^{(3)}=0.34$ ). Comparing Figs. 14 and 15, we see that the negative effective-mass ridges in the photon dispersion give rise to corresponding repulsive positive ridges in the exciton energy. However, these repulsive ridges lead to a sharp local minimum at  $\vec{q}=0$  in the dressed exciton dispersion. Therefore, an exciton can be captured with a strongly renormalized positive effective-mass at  $\vec{q}=0$ . The exact photonic dispersion also exhibits positive effective-mass local minima at  $\vec{q}=[0.5, 0], [-0.5, 0], [0, 0.5], [0, -0.5]$ . An exciton interacting with these positive effective-mass modes will be dressed and captured at these wave vectors. Depending on specific PBG-QW heterostructure and choice of QW insertion position, the global minimum of the exciton dispersion could occur at either the  $\vec{q}=0$  local minimum or  $\vec{q}=[0.5, 0]$ , etc., local minima. For an exciton is captured at the wave vector  $[0, 0]$ , Fig. 16 shows the renormalized exciton effective mass as a function of the detuning between the bare exciton recombination energy and 3D lower band edge. At  $\vec{q}=0$ , the renormalized exciton effective mass is still about 3 orders of magnitude less than the electron mass.

## V. INFLUENCE OF STATIC DISORDER AND PHONONS

Our results on exciton dressing and capture from the previous section are based on models satisfying the conservation of the exciton in-plane momentum. Nevertheless, most of our conclusions are robust to the presence of disorder and weak random scattering in the sample, provided that this disorder is not so strong as to seriously modify the electromagnetic mode structure in the vicinity of the exciton recombination energy. In real systems, disorder may arise from the presence of impurities in the QW plane and the roughness at the QW interface. In the case of a layer of quantum dots, randomness arises from the size distribution and positioning of the dots. Each of these forms of disorder breaks the in-plane translational symmetry. The energy fluctuation is typically small compared to the exciton binding energy, so the internal degrees of freedom of the exciton (as a bound

electron-hole state) are not affected by the weak disorder. The exciton's center-of-mass (COM) motion, however, experiences a weak static random potential on top of the strong periodic potential.<sup>37</sup> A model Hamiltonian describing the motion of the exciton COM is given by

$$H = -\frac{\hbar^2 \nabla_R^2}{2M} + V(R). \quad (30)$$

Here,  $M$  is the bare exciton effective mass.  $V(R)$  is a random potential acting on the exciton COM. It is assumed to have a Gaussian autocorrelation with root mean square (rms) amplitude  $\Delta$  and correlation length  $\Lambda$ :

$$\langle V(R_1)V(R_2) \rangle = \Delta^2 e^{-|R_1 - R_2|^2/\Lambda^2}. \quad (31)$$

It is straightforward to show that the rms scattering matrix element  $\langle |V_{\vec{K}, \vec{K}'}|^2 \rangle$  for the transition from an exciton state  $|\vec{K}\rangle$  to another state  $|\vec{K}'\rangle$  is proportional to Fourier transform the correlation function [Eq. (31)] evaluated at  $\vec{P}=\vec{K}-\vec{K}'$ . In  $d$ -spatial dimensions,

$$\langle |V_{\vec{K}, \vec{K}'}|^2 \rangle \propto \Delta^2 \Lambda^d e^{-\Lambda^2 P^2/4}. \quad (32)$$

If the dressed exciton effective mass becomes  $s^2 M$ , in which  $s$  is a scaling factor, the exciton dynamics is governed by the new effective Hamiltonian  $H' = -\frac{\hbar^2 \nabla_{R'}^2}{2s^2 M} + V(R) = -\frac{\hbar^2 \nabla_{R'}^2}{2M} + V'(R')$ , where  $R' \equiv sR$  and  $V'(R') = V(R'/s)$ . Using the disorder autocorrelation function [Eq. (31)], we obtain

$$\langle V'(R'_1)V'(R'_2) \rangle = \Delta^2 e^{-|R'_1 - R'_2|^2/(s\Lambda)^2}. \quad (33)$$

Clearly, the disorder induced scattering of the dressed exciton is the same as that of the bare exciton except with disorder correlation length of  $s\Lambda$  rather than  $\Lambda$ . For typical disorder on the scale of nanometers and  $P$  on the scale of a photon wave vector,  $(\Lambda P)^2 \ll 1$ . In the two-dimensional ( $d=2$ ) plane of the QW, it follows from Eq. (32) that the rms scattering matrix elements for the dressed exciton are modified by a factor of  $s^2$ . In other words, as the exciton effective mass becomes smaller, the rms scattering amplitude due to short-range-correlated disorder becomes proportionately smaller. Equivalently, the high mobility of the dressed exciton causes significant spatial averaging over the disorder potential, thereby reducing any deleterious effects of random scattering. This type of motional narrowing of the exciton spectral line has been extensively studied<sup>37-41</sup> in other contexts. The captured exciton in the PBG-QW heterostructure has a typical effective-mass reduction of  $10^{-4}$ . Due to the motional narrowing effect, this highly mobile dressed exciton is robust to the effects of static disorder on the electronic scale. The dressed exciton dispersion may, nevertheless, be influenced by larger scale disorder that alters the overall photonic band structure or closes the PBG. In order to avoid this possibility, the PBG cladding regions should be fabricated to a resolution of at least 50 nm.

The robustness of the dressed exciton to nonradiative scattering and decay effects is also an important issue for experimental observation of the effects we predict. While a typical PBG of heterostructures with gap centered at  $1.5 \mu\text{m}$  is about 100 meV, the longitudinal optical (LO) phonon en-

ergy can be roughly 30–40 meV in III-V semiconductors.<sup>42</sup> In this situation, at low temperature (thermal energy below the LO phonon energy), the exciton can decay by simultaneous emission of a lower frequency photon (below the PBG) and one or more LO phonons. Starting from Fröhlich model of electron-LO phonon interaction,<sup>43</sup> the matrix element describing the exciton (composed of a conduction band electron and a valence hole) scattering through emission or absorption of a LO phonon with wave vector  $\vec{q}$  and  $k_z$  is the following:

$$V_{q,k_z} \propto \langle \Psi_{\vec{k}_1, \lambda_1} | e^{i(\vec{q}\cdot\vec{r}_e + k_z z_e)} - e^{i(\vec{q}\cdot\vec{r}_h + k_z z_h)} | \Psi_{\vec{k}_2, \lambda_2} \rangle / (q^2 + k_z^2)^{1/2}. \quad (34)$$

This describes the exciton transition from  $\Psi_{\vec{k}_1, \lambda_1}$  to  $\Psi_{\vec{k}_2, \lambda_2}$  with wave vector change  $\vec{q}$ . The wave vectors  $\vec{k}_{1,2}$  characterize the exciton COM motion and  $\lambda$  characterizes the exciton internal degrees of freedom.  $\vec{r}_e$  and  $\vec{r}_h$  are electron and hole coordinates. Defining  $\alpha_e = m_e^*/(m_e^* + m_h^*)$  and  $\alpha_h = m_h^*/(m_e^* + m_h^*)$ , we transform to the COM coordinate  $\vec{R}$  and the relative electron-hole separation coordinate  $\vec{r}$ . In this case,  $\vec{r}_e = \vec{R} + \alpha_h \vec{r}$  and  $\vec{r}_h = \vec{R} - \alpha_e \vec{r}$ . Performing the integral over  $\vec{R}$ , we obtain the in-plane momentum conservation  $\vec{k}_1 = \vec{k}_2 + \vec{q}$ . Assuming that the electron and hole wave functions along the normal direction are given by the ground state of a particle in 1D box [see Eq. (4b) with  $m=1$ ], we can perform the integral over  $z_e$  and  $z_h$  to obtain a form factor  $F(k_z) \equiv \int dz |f_{(c,v)}(z)|^2 e^{ik_z z}$  describing QW confinement of the charge carriers. Equation (34) then becomes

$$V_{q,k_z} \propto \delta_{\vec{k}_1, \vec{k}_2 + \vec{q}} F(k_z) \langle \phi_{\lambda_1} | e^{i\alpha_h \vec{q}\cdot\vec{r}} - e^{-i\alpha_e \vec{q}\cdot\vec{r}} | \phi_{\lambda_2} \rangle / (q^2 + k_z^2)^{1/2}. \quad (35)$$

Here,  $\phi$  is wave function of electron and hole relative coordinates. Before we perform the integral over  $\vec{r}$ , we first qualitatively analyze the nature of this matrix element for small  $q$ . For this purpose, we perform a Taylor expansion of the exponentials and keep up to the second order terms. This yields  $e^{i\alpha_h \vec{q}\cdot\vec{r}} - e^{-i\alpha_e \vec{q}\cdot\vec{r}} \simeq i\vec{q}\cdot\vec{r} - \frac{m_h^* - m_e^*}{m_h^* + m_e^*} (\vec{q}\cdot\vec{r})^2 / 2$ . Here, the zeroth order is canceled out because of opposite charge of electron and hole. If the parity of relative electron and hole movement is changed by LO scattering, the leading term (first order) is  $i\vec{q}\cdot\vec{r}$ . Otherwise, the leading term will be the second order term  $-\frac{m_h^* - m_e^*}{m_h^* + m_e^*} (\vec{q}\cdot\vec{r})^2 / 2$ . Assuming that the exciton internal degrees of freedom are not changed by the LO phonon scattering (exciton remains in the lowest  $1s$  state), for small  $q$ , we qualitatively have

$$V_{q,k_z} \propto \frac{q^2}{\sqrt{|q|^2 + k_z^2}}. \quad (36)$$

Using the explicit exciton  $1s$  wave function [given by Eq. (3c)], we can perform the integral over  $\vec{r}$  to obtain

$$V_{q,k_z} \propto \delta_{\vec{k}_1, \vec{k}_2 + \vec{q}} F(k_z) [G_h(q) - G_e(-q)] / (q^2 + k_z^2)^{1/2}, \quad (37)$$

where  $G_{e,h}(q) = \left[ \left( \frac{\alpha_{e,h} q a_B}{4} \right)^2 + 1 \right]^{-3/2}$ . This is in agreement with Eq. (36) for small  $q$ .

The decay of the dressed exciton by emission of a single photon and a single LO phonon is severely limited by the requirements of energy and momentum conservation. In the dressed state, the exciton wave vector is that of a band-edge photon. Since the emitted photon also has a small wave vector, it follows that emitted phonon must have wavelength comparable to that of the emitted light. However, from the coupling constant [Eq. (37)], we have shown that  $V_{q,k_z} \propto \frac{q^2}{\sqrt{|q|^2 + k_z^2}}$  for  $q \ll \frac{1}{a_B}$ . Therefore, the transition matrix element for single-phonon-assisted decay of the dressed exciton captured by a photonic band edge is very small. By way of contrast, the bare (untrapped) exciton can propagate over a broad range of initial wave vectors. In this case, LO-phonon-assisted decay (with a broad range of phonon wave vectors) is much more probable. For the dressed exciton, on the other hand (trapped by a photonic band edge), phonon-assisted decay requires two or more LO phonons to simultaneously satisfy momentum conservation and occur with stronger coupling.

If we consider LO phonon processes that change the exciton internal degree of freedom, we have to consider higher order perturbation theory involving more intermediate states. Theoretical evaluation of the multiphonon processes is complicated because of multiple summation over intermediate states such as the exciton internal states and LO phonon states. However, even in the strongly ionic semiconductors, the Fröhlich exciton-phonon polar interaction turns out to be a weak interaction and the intensities of the multiphonon luminescence lines strongly decrease with increasing number of participating phonons.<sup>44,45</sup> Nakajima *et al.*<sup>46</sup> show that the instantaneous interaction between the exciton and phonons will more or less be averaged out by rapid translational motion of the exciton. This leads to the motional narrowing of the overall width of the exciton absorption spectra and motional reduction of the phonon sideband intensities. This is the same mechanism that we described in the case of exciton scattering by a static random potential. In summary, weak electron-phonon coupling (due to momentum conservation) and motional narrowing provide robustness and stability to the dressed exciton.

## VI. CONCLUSION

In this paper, we have demonstrated the possibility of novel exciton dynamics in a PBG-QW heterostructure, mediated by an engineered electromagnetic vacuum. In a PBG, the exciton cannot decay directly by single-photon radiative recombination and the exciton is endowed with a long lifetime. Nevertheless, strong coupling is possible to slightly off-resonance band-edge photons. By emitting and reabsorbing the virtual photons near the edge of the PBG, the exciton dispersion is fundamentally changed. This effect is most dramatic when the exciton wave vector and recombination energy nearly coincide with a photonic band edge. The exciton becomes strongly dressed and “trapped” by this band-edge photon. The renormalized dispersion of this dressed exciton has a significant local energy minimum (1–10 meV) at the photonic band-edge wave vector. Due to strong dressing by

the band-edge photon, the exciton's effective mass is comparable to the photon effective mass (4–5 orders less in magnitude of the bare electron mass). Once the exciton equilibrates and falls into this local minimum, the dressed exciton become highly mobile. This, in turn, makes the exciton immune to the influence of LO phonon and disorder through “motional narrowing.” The “half light” and “half matter” nature of the dressed exciton decreases its coupling with LO phonon and disorder.

Our detailed numerical results demonstrate that radiative hopping through RDDI for a QW exciton in PBG material is a dominant transport mechanism as the exciton recombination energy and momentum approach that of a photonic band edge. The resulting renormalized exciton dispersion relation is almost independent of the original bare exciton hopping from conventional charge transport. This implies that our mechanism for dressed exciton dynamics applies not only to a QW layer but also to a layer of quantum dots placed within a 3D PBG material. Our mechanism for the exciton dressed state relies on coherent emission and reabsorption of virtual band-edge photons. The coherence of this process is likely to appear at temperature scales ( $\lesssim 100$  K) defined by the depth of the dressed exciton dispersion minima. The drastic decrease of the dressed exciton effective mass may facilitate observation of high temperature many-body coherence effects, such as Bose-Einstein condensation (BEC) in a finite 2D system [ $T_c \propto m^{-1}$  (Ref. 47)] or a 2D harmonic trapped system [ $T_c \propto m^{-1/2}$  (Ref. 47)]. Here, the transition critical temperature  $T_c$  from the normal (incoherent) state to the BEC strongly depends on the exciton effective mass  $m$ . The half light nature of the dressed exciton also makes the heterostructure promising for the development of extremely low threshold lasers, in which the quantum statistics of the emitted photons mirrors the quantum statistics of the many-body state of dressed excitons.<sup>15</sup>

#### ACKNOWLEDGMENTS

We are grateful to Alongkarn Chutinan for discussions on numerical calculations. This work was supported in part by the Natural Sciences and Engineering Research Council of Canada, the Government of Ontario Premier's Platinum Grant, and the Canadian Institute of Advanced Research.

#### APPENDIX: EXCITON-PHOTON INTERACTION IN A PHOTONIC CRYSTAL

In this appendix, we describe the coupling between a QW exciton and electromagnetic modes in a PBG heterostructure. Consider the Hamiltonian for  $N$  interacting electrons in a semiconductor:

$$H_e = \sum_i \left( -\frac{\hbar^2}{2m} \right) \nabla_i^2 + \frac{1}{2} \sum_{i \neq j} \frac{e^2}{|\vec{r}_i - \vec{r}_j|} - \sum_{i,l} \frac{Ze^2}{|\vec{r}_i - \vec{R}_l|}. \quad (\text{A1})$$

Here,  $i$  and  $l$  refer to the index of the electron and nuclei, respectively, and  $Z$  indicates the nuclear charge. We consider a two-band semiconductor model, whose many-electron ground state takes the form of a Slater determinant:

$$\Psi_0 = \mathcal{A} \{ \psi_{v\vec{k}_1}, \psi_{v\vec{k}_2}, \dots, \psi_{v\vec{k}_i}, \dots, \psi_{v\vec{k}_N} \}. \quad (\text{A2})$$

Here,  $\mathcal{A}$  is the antisymmetrizing operator,  $N$  is the number of unit cells, and  $\psi_{v\vec{k}_i}$  are one-electron wave functions in the valence band of the semiconductor. Equation (3a) shows the exciton state vector in second quantized form. In first quantization, the exciton state with wave vector  $k_{ex}$  can then be expanded in the following form:

$$\Psi_{\vec{k}_{ex}} = \sum_{\vec{k}} A_{\vec{k}, \vec{k}_{ex}} \Phi_{(c, \vec{k} + (1/2)\vec{k}_{ex}), (v, \vec{k} - (1/2)\vec{k}_{ex})}, \quad (\text{A3a})$$

$$\begin{aligned} & \Phi_{(c, \vec{k} + (1/2)\vec{k}_{ex}), (v, \vec{k} - (1/2)\vec{k}_{ex})} \\ &= \mathcal{A} \{ \psi_{v\vec{k}_1}, \psi_{v\vec{k}_2}, \dots, \psi_{c, \vec{k} + (1/2)\vec{k}_{ex}}, \dots, \psi_{v\vec{k}_N} \}. \end{aligned} \quad (\text{A3b})$$

Here,  $A_{\vec{k}, \vec{k}_{ex}}$ , defined by Eq. (3b), is the Fourier transform of electron and hole relative wave functions. In Eq. (A3b), the valence band one-electron wave function at wave vector  $-\frac{1}{2}\vec{k}_{ex}$  has been removed and replaced with a conduction band one-electron wave function  $\psi_{c, \vec{k} + (1/2)\vec{k}_{ex}}$  with wave vector  $\vec{k} - \frac{1}{2}\vec{k}_{ex}$ , where  $\vec{k}_{ex}$  is the exciton center-of-mass wave vector. The energy difference between an exciton state [Eq. (A3a)] and ground state [Eq. (A2)] is

$$\varepsilon_{k_{ex}} = \varepsilon_b + \frac{\hbar^2 k_{ex}^2}{2(m_e^* + m_h^*)}, \quad (\text{A4})$$

where  $\varepsilon_b$  is the binding energy of the exciton. Since we consider an exciton confined to a QW,  $k_{ex}$  is the exciton's 2D wave vector along the plane.  $m_e^*$  and  $m_h^*$  are the effective masses of the electron and hole, respectively.

The interaction Hamiltonian of electrons coupled to an electromagnetic Bloch wave is given by the expression

$$H_i = \frac{e}{2m_e} \sum_{i=1}^N [\hat{A}(\vec{r}_i) \cdot \hat{p}_i + \hat{p}_i \cdot \hat{A}(\vec{r}_i)]. \quad (\text{A5a})$$

Here, the quantized vector potential for a single photonic mode with wave vector  $k_{pt}$  is

$$\hat{A}(\vec{r}) = (\hbar/2\epsilon_0\omega_{k_{pt}}V)^{1/2} [\vec{u}(\vec{r})e^{i\vec{k}_{pt}\vec{r}}c_{k_{pt}} + \vec{u}^*(\vec{r})e^{-i\vec{k}_{pt}\vec{r}}c_{k_{pt}}^\dagger], \quad (\text{A5b})$$

where the normalized mode function  $\vec{u}(\vec{r})$  is defined in Sec. II A.  $c$  and  $c^\dagger$  are photon annihilation and creation operators, respectively.

The coupling constant  $g$  for the second quantized exciton-photon interaction is defined through the transition matrix element  $T \equiv \langle \Psi_{\vec{k}_{ex}} | 0^{photon} | H_i | \Psi_0, 1_{k_{pt}}^{photon} \rangle = i\hbar g$ . The transition matrix element from  $\Psi_0$  to  $\Psi_{\vec{k}_{ex}}$ , obtained by annihilating a photon with wave vector  $\vec{k}_{pt}$ , can be rewritten as

$$T = \langle \Psi_{\vec{k}_{ex}} | 0^{photon} | \frac{e}{2} \sum_{i=1}^N \left[ \hat{A}(\vec{r}_i) \cdot \frac{1}{i\hbar} [\vec{r}_i, H_e] + \frac{1}{i\hbar} [\vec{r}_i, H_e] \cdot \hat{A}(\vec{r}_i) \right] \rangle \times |\Psi_0, 1_{\vec{k}_{pt}}^{photon}\rangle. \quad (\text{A6})$$

Here, we have used the commutation relationship  $\frac{\hat{p}_i}{m_e} = \frac{1}{i\hbar} [\vec{r}_i, H_e]$ .

In a spatially homogeneous  $[\epsilon(\vec{r}) = \text{constant}]$  dielectric,  $[H_e, \hat{A}(\vec{r}_i)] = 0$  upon quantizing the electric field in transverse plane waves and using the Coulomb gauge  $\vec{\nabla} \cdot [\epsilon(\vec{r}) \vec{A}] = 0$ . Then, Eq. (A5a) reduces to a simple form of the minimal coupling Hamiltonian. However, this is not the case in PBG materials with strong dielectric variations  $[\epsilon(\vec{r}) \neq \text{constant}]$ . We may, nevertheless, assume that the electromagnetic field varies little over the spatial extent of the electronic wave function, allowing us to set  $[H_e, \hat{A}(\vec{r}_i)] \approx 0$ . Using the commutation approximation, Eq. q. (A6) reduces to  $g = e\epsilon_{\vec{k}_{ex}} (\hbar/2\epsilon_0\omega_{\vec{k}_{pt}} V)^{1/2} \vec{g}$ , where

$$\vec{g} = \langle \Psi_{\vec{k}_{ex}} | \sum_{i=1}^N \vec{u}(\vec{r}_i) e^{i\vec{k}_{pt}\vec{r}_i} \cdot \vec{r}_i | \Psi_0 \rangle. \quad (\text{A7})$$

Substituting Eq. (A3a) into Eq. (A7) and then evaluating the matrix element of the sum of one-particle operators between determinantal states yield

$$\vec{g} = \sum_{\vec{k}} A_{\vec{k}, \vec{k}_{ex}} \langle \psi_{c, \vec{k} + (1/2)\vec{k}_{ex}} | \vec{u}(\vec{r}) e^{i\vec{k}_{pt}\vec{r}} \cdot \vec{r} | \psi_{v, \vec{k} - (1/2)\vec{k}_{ex}} \rangle \quad (\text{A8})$$

Substituting the one-electron wave functions given by Eqs. (4a) and (4b) for the case  $m=1$  into Eq. (A8), we obtain

$$\vec{g} = \sum_{\vec{k}} A_{\vec{k}, \vec{k}_{ex}} \int h(\rho, z) d\rho dz. \quad (\text{A9})$$

Here,

$$h(\rho, z) = f_c^*(z) u_{\Gamma_c}^*(\vec{r}) e^{i(\vec{k}_{pt} - \vec{k}_{ex}) \cdot \vec{\rho} + ik_z z} [e^{\vec{r}} \cdot \vec{u}(\vec{r})] u_{\Gamma_v}(\vec{r}) f_v(z) / S$$

and the integration is over the volume of the quantum well layer. Performing the integral over the rapidly varying (electronic) coordinates in  $u_{\Gamma_c}^*(\vec{r})$  and  $u_{\Gamma_v}(\vec{r})$ , we have

$$\vec{g} = \sum_{\vec{k}} A_{\vec{k}, \vec{k}_{ex}} \vec{d} \cdot \int \vec{h}_1(\rho, z) d\rho dz. \quad (\text{A10})$$

Here,  $\vec{d} = \langle u_{\Gamma_c}(\vec{r}) | e^{\vec{r}} | u_{\Gamma_v}(\vec{r}) \rangle$  is the exciton dipole moment and  $\vec{h}_1(\rho, z) = f_c^*(z) e^{i(\vec{k}_{pt} - \vec{k}_{ex}) \cdot \vec{\rho} + ik_z z} \vec{u}(\vec{r}) f_v(z) / S$ , where  $S$  is the quan-

tum well area. Using Eq. (4b) for the case of  $m=1$ , we note that  $\int f_c^*(z) f_v(z) dz = 1$ . Since the exciton is confined in the QW, we assume the QW position is at  $z_0$  to obtain

$$\vec{g} = e^{ik_z z_0} \sum_{\vec{k}, G_{\parallel}^n} A_{\vec{k}, \vec{k}_{ex}} \delta_{\vec{k}_{ex}, \vec{k}_{pt} + G_{\parallel}^n} \vec{d} \cdot \vec{u}_{G_{\parallel}^n}. \quad (\text{A11})$$

Here, we have used Eq. (2) to obtain  $\sum_n \delta_{\vec{k}_{ex}, \vec{k}_{pt} + G_{\parallel}^n} \vec{u}_{G_{\parallel}^n} = S^{-1} \int e^{i(\vec{k}_{pt} - \vec{k}_{ex}) \cdot \vec{\rho}} \vec{u}(\rho, z_0) d\rho$ , where  $S$  is the QW area. From Eq. (3b), we find  $\sum_{\vec{k}} A_{\vec{k}, \vec{k}_{ex}} = \phi(0) S^{1/2}$ , where  $\phi(0)$  is the amplitude for the electron and hole coordinates to coincide. We finally obtain

$$g = e\epsilon_{\vec{k}_{ex}} (\hbar/2\epsilon_0\omega_{\vec{k}_{pt}} l)^{1/2} e^{ik_z z_0} \phi(0) \sum_{G_{\parallel}^n} \delta_{\vec{k}_{pt}, \vec{k}_{ex} + G_{\parallel}^n} \vec{d} \cdot \vec{u}_{G_{\parallel}^n}, \quad (\text{A12})$$

where  $l$  is the length (in the  $z$  direction) of the quantization box (containing the PBG QW heterostructure). From Eq. (A12), we obtain the interaction Hamiltonian in second quantized form:

$$H_i = \sum_{\vec{k}_{ex}, \vec{k}_{pt}} i\hbar (g B_{\vec{k}_{ex}}^{\dagger} c_{\vec{k}_{pt}} - g^* B_{\vec{k}_{ex}} c_{\vec{k}_{pt}}^{\dagger}), \quad (\text{A13})$$

where  $B_{\vec{k}_{ex}}^{\dagger}$  creates a  $1s$  exciton with COM wave vector  $\vec{k}_{ex}$ . From Eq. (A12), we see that the exciton and photon quasi-wave-vectors in the plane ( $\vec{k}_{ex}$  and  $\vec{k}_{pt_{\parallel}}$ ) are conserved modulo of a reciprocal lattice vector  $G_{\parallel}^n$ . We can redefine  $\vec{q} \equiv \vec{k}_{ex} \equiv \vec{k}_{pt_{\parallel}}$ . Depending on the exciton wave vector direction, we can decompose the exciton dipole matrix element  $\vec{d} = \langle u_{\Gamma_c}(\vec{r}) | e^{\vec{r}} | u_{\Gamma_v}(\vec{r}) \rangle$  into three orthogonal directions. If the dipole polarization is in the QW plane and perpendicular to the exciton wave vector, this exciton is called a T exciton. If the dipole polarization is in the QW plane and parallel to the exciton wave vector, it is called an L exciton. If the dipole is polarized along the normal  $z$  direction, it is called a Z exciton. Likewise, the electromagnetic field pattern can be decomposed into corresponding directions as well. By denoting  $j \equiv (\text{T}, \text{L}, \text{Z})$ , considering many photonic bands characterized by band index  $p$  and assuming  $z_0 = 0$ , the interaction Hamiltonian can be written as

$$H_i = \sum_{j, n, p, k_z} i\hbar g_{j, n, p} B_{j, \vec{q} + G_{\parallel}^n}^{\dagger} c_{p, (q, k_z)} + \text{H.c.}, \quad (\text{A14a})$$

$$g_{j, n, p} = - \frac{\epsilon_{j, \vec{q} + G_{\parallel}^n}}{\hbar \sqrt{2\hbar \omega_{p, (\vec{q}, k_z)}} \epsilon_0 l} \phi(0) d_j u_{j, n, p}. \quad (\text{A14b})$$

<sup>1</sup>S. John, Phys. Rev. Lett. **58**, 2486 (1987).

<sup>2</sup>E. Yablonovitch, Phys. Rev. Lett. **58**, 2059 (1987).

<sup>3</sup>S. John, Phys. Rev. Lett. **53**, 2169 (1984).

<sup>4</sup>S. John and J. Wang, Phys. Rev. Lett. **64**, 2418 (1990).

<sup>5</sup>S. John and J. Wang, Phys. Rev. B **43**, 12772 (1991).

<sup>6</sup>S. John and T. Quang, Phys. Rev. A **50**, 1764 (1994).

<sup>7</sup>M. Florescu and S. John, Phys. Rev. A **64**, 033801 (2001).

<sup>8</sup>S. John and T. Quang, Phys. Rev. Lett. **76**, 1320 (1996).

<sup>9</sup>S. John and T. Quang, Phys. Rev. Lett. **76**, 2484 (1996).

<sup>10</sup>S. John and T. Quang, Phys. Rev. A **54**, 4479 (1996).

- <sup>11</sup>V. P. Bykov, *Sov. J. Quantum Electron.* **4**, 861 (1975).
- <sup>12</sup>J. J. Hopfield, *Phys. Rev.* **112**, 1555 (1958).
- <sup>13</sup>L. C. Andreani, in *Confined Electrons and Photons: New Physics and Applications*, edited by E. Burstein and C. Weisbuch (Plenum, New York, 1995).
- <sup>14</sup>D. S. Citrin, in *Confined Electrons and Photons: New Physics and Applications*, edited by E. Burstein and C. Weisbuch (Plenum, New York, 1995).
- <sup>15</sup>H. Deng, G. Weihs, D. Snoke, J. Bloch, and Y. Yamamoto, *Proc. Natl. Acad. Sci. U.S.A.* **100**, 15318 (2003).
- <sup>16</sup>E. Giacobino, J.-P. Karr, A. Baas, G. Messin, M. Romanelli, and A. Bramati, *Solid State Commun.* **134**, 97 (2005).
- <sup>17</sup>F. Marchetti, M. Szymanska, P. Eastham, B. Simons, and P. Littlewood, *Solid State Commun.* **134**, 111 (2005).
- <sup>18</sup>F. P. Laussy, G. Malpuech, A. Kavokin, and P. Bigenwald, *Solid State Commun.* **134**, 121 (2005).
- <sup>19</sup>L. C. Andreani, D. Gerace, and M. Agio, *Phys. Status Solidi B* **242**, 2197 (2005).
- <sup>20</sup>D. P. Craig and T. Thirunamachandran, *Molecular Quantum Electrodynamics: An Introduction to Radiation-Molecule Interactions* (Academic, New York, 1984).
- <sup>21</sup>O. Toader and S. John, *Science* **292**, 1133 (2001).
- <sup>22</sup>K. Ho, C. Chan, C. Soukoulis, R. Biswas, and M. Sigalas, *Solid State Commun.* **89**, 413 (1994).
- <sup>23</sup>A. Blanco *et al.*, *Nature (London)* **405**, 437 (2000).
- <sup>24</sup>S. R. Kennedy, M. J. Brett, O. Toader, and S. John, *Nano Lett.* **2**, 59 (2002).
- <sup>25</sup>N. Tetreault, G. von Freymann, M. Deubel, M. Hermatschweiler, F. Perez-Willard, S. John, M. Wegener, and G. A. Ozin, *Adv. Mater. (Weinheim, Ger.)* **18**, 457 (2006).
- <sup>26</sup>J. Schilling, F. Müller, S. Matthias, R. B. Wehrspohn, and U. Gösele, *Appl. Phys. Lett.* **78**, 1180 (2001).
- <sup>27</sup>S. Noda, A. Chutinan, and M. Imada, *Nature (London)* **407**, 608 (2000).
- <sup>28</sup>S. Noda, M. Imada, M. Okano, S. Ogawa, M. Mochizuki, and A. Chutinan, *IEEE J. Quantum Electron.* **38**, 726 (2002).
- <sup>29</sup>S. Noda, K. Tomoda, N. Yamamoto, and A. Chutinan, *Science* **289**, 604 (2000).
- <sup>30</sup>S. Y. Lin, J. G. Fleming, D. L. Hetherington, B. K. Smith, R. Biswas, K. M. Ho, M. M. Sigalas, W. Zubrzycki, S. R. Kurtz, and J. Bur, *Nature (London)* **394**, 251 (1998).
- <sup>31</sup>O. Toader and S. John, *Phys. Rev. E* **66**, 016610 (2002).
- <sup>32</sup>S. Ogawa, M. Imada, S. Yoshimoto, M. Okano, and S. Noda, *Science* **305**, 227 (2004).
- <sup>33</sup>V. Savona, Z. Hradil, A. Quattropani, and P. Schwendimann, *Phys. Rev. B* **49**, 8774 (1994).
- <sup>34</sup>O. Madelung, *Introduction to Solid-State Theory* (Springer, Berlin, 1978).
- <sup>35</sup>J. M. Ziman, *Elements of Advanced Quantum Theory* (Cambridge University Press, London, 1969).
- <sup>36</sup>C. Weisbuch, M. Nishioka, A. Ishikawa, and Y. Arakawa, *Phys. Rev. Lett.* **69**, 3314 (1992).
- <sup>37</sup>R. Zimmerman, *Phys. Status Solidi B* **173**, 129 (1992).
- <sup>38</sup>P. K. Basu, *Phys. Rev. B* **44**, 8798 (1991).
- <sup>39</sup>D. M. Whittaker, P. Kinsler, T. A. Fisher, M. S. Skolnick, A. Armitage, A. M. Afshar, M. D. Sturge, J. S. Roberts, G. Hill, and M. A. Pate, *Phys. Rev. Lett.* **77**, 4792 (1996).
- <sup>40</sup>V. Savona, C. Piermarocchi, A. Quattropani, F. Tassone, and P. Schwendimann, *Phys. Rev. Lett.* **78**, 4470 (1997).
- <sup>41</sup>D. M. Whittaker, *Phys. Rev. Lett.* **80**, 4791 (1998).
- <sup>42</sup>S. Adachi, *Physical Properties of III-V Semiconductor Compounds: InP, InAs, GaAs, GaP, InGaAs, and InGaAsP* (Wiley, New York, 1992).
- <sup>43</sup>H. Fröhlich, *Adv. Phys.* **3**, 325 (1954).
- <sup>44</sup>S. Permogorov, in *Excitons*, edited by E. I. Rashba and M. D. Sturge (North-Holland, Amsterdam, 1982).
- <sup>45</sup>A. Klochikhin, S. Permogorov, and A. Reznitsky, *Sov. Phys. JETP* **44**, 1176 (1976).
- <sup>46</sup>S. Nakajima, Y. Toyozawa, and R. Abe, *Sov. Phys. JETP* **44**, 1176 (1976).
- <sup>47</sup>C. Pethick and H. Smith, *Bose-Einstein Condensation in Dilute Gases* (Cambridge University Press, Cambridge, England, 2002).